





Carbonate platform drowning caught in the act: The sedimentology of Saya de Malha Bank (Indian Ocean)

CHRISTIAN BETZLER* , SEBASTIAN LINDHORST* , JOHN J. G. REIJMER†‡ ,
JUAN CARLOS BRAGA§ , THOMAS LÜDMANN*, OR M. BIALIK¶, JESUS REOLID§,
ANNA-LENA GEßNER**, DAGMAR HAINBUCHER†† and DASS BISSESSUR‡‡

*Institut für Geologie, Universität Hamburg, Bundesstr. 55, 20146 Hamburg, Germany (E-mail: christian.betzler@uni-hamburg.de)

†Department of Geosciences, Faculty of Science, Vrije Universiteit Amsterdam, De Boelelaan 1085, 1081 HV Amsterdam, The Netherlands

‡Reijmer GeoConsulting, Amstelveen, The Netherlands

§Departamento de Estratigrafía y Paleontología, Facultad de Ciencias, Avenida de la Fuente Nueva S/N, 18071 Granada, Spain

¶Department of Geosciences, Faculty of Science, University of Malta, Msida MSD 2080, Malta

**Center for Marine Sensors, Institute for Chemistry and Biology of the Marine Environment, Universität Oldenburg, Schleusenstraße 1, 26382 Wilhelmshaven, Germany

††Institut für Meereskunde, Universität Hamburg, Bundesstr. 53, 20146 Hamburg, Germany

‡‡Department for Continental Shelf, Maritime Zones Administration & Exploration, 12 Intendance Street, Port-Louis 11328, Mauritius

Associate Editor – Jody Webster

ABSTRACT

Mesophotic reefs, hardgrounds and current-controlled pelagic to hemipelagic carbonates are facies marking carbonate platform drowning successions, irrespective of the factors controlling this evolution. A modern analogue of a carbonate platform in a state of drowning, where these facies occur has not been properly reported on to date. In the present study, the sedimentary environments of the Saya de Malha Bank are characterized using a multi-disciplinary approach including sedimentology, hydroacoustics, seismics and oceanography. The Saya de Malha Bank edifice with a surface of 40 808 km² is located in the tropical Indian Ocean and lies in a water depth of 8 to 300 m extending from the surrounding more than 2000 m deep ocean floor, with no reef reaching the sea surface. Mesophotic coral and red algal facies co-exist with hemipelagic and bioclastic sands, together with a hardground. Ocean currents and internal waves are identified as major sedimentological controlling factors in the absence of elevated nutrient influx. Many features distributed along the present-day Saya de Malha Bank were described from studies presenting fossil examples of carbonate platform drowning. The results herein can therefore be applied to other drowning examples, in some cases allowing for more accurate interpretation of the stratigraphic record.

Keywords Internal waves, Mascarene Plateau, mesophotic reefs, South Equatorial Current.

INTRODUCTION

Carbonate platform drowning, i.e. the sudden to gradual demise of a shallow-water carbonate

factory, is common in the geological record. Eustatic sea-level changes, variations in subsidence rates and environmental effects have been identified as controlling factors for such a

development (Schlager, 2005). Regardless of the drowning trigger, the stratigraphic record of this process is comparable and often characterized by either a drowning sequence or a drowning unconformity (Schlager, 2005). Triple facies compound usually make up such a stratigraphic element, with: (i) mesophotic reefs witnessing the initial stage of deepening below the upper euphotic zone; (ii) a hardground marking the interruption of neritic carbonate deposition; and (iii) current-deposited pelagic and hemipelagic carbonate ooze indicating that the drowned platform is positioned in the path of ocean currents. Carbonate ooze may be replaced by or mixed with clays if the carbonate platform lies on a continental shelf or in a zone with siliciclastic influx (Schlager, 1989, 2005).

The interpretation of a drowning sequence or unconformity in the geological record and the full understanding of how the associated facies are related to one another is, however, hampered by the absence of a well-described modern analogue of a carbonate platform in a state of early drowning. The shallow-water production areas of many carbonate platforms in the Indo-Pacific, for example, shrunk during the Neogene and Quaternary (Montaggioni, 2005; Droxler & Jorry, 2021) but platform parts are still occupied by reefs growing to sea level. The Mascarene Plateau in the Indian Ocean appears to be an exception as it displays various co-existing facies, with the shallowest reefs lying at a water depth of 7 to 8 m (Vortsepneva, 2008) on the 40 808 km² large Saya de Malha Bank. Latter appears to be a natural laboratory to analyse lateral facies variations of a carbonate platform which is in the state of drowning. Further possible candidates to study early drowning features in the future for example would be Saba Bank (1850 km²; Caribbean) with a platform top at 10 to 50 m water depth bathed in the strong Westward Caribbean surface water current (Van der Land, 1977), the Pee Shoal (Indonesia) at water depths of 20 m and more (Wienberg *et al.*, 2010) or the submerged reefs within the Gulf of Carpenteria (Australia); interpreted to be in the catch-up phase (Harris *et al.*, 2004).

Using sedimentological, hydroacoustic and seismic data it will be shown how the different facies known from drowning sequences in the geological record are laterally arranged on Saya de Malha Bank. Ocean seismics further elucidate the contribution of currents and internal waves (IW) impinging on such an edifice.

STUDY AREA

The Mascarene Plateau is an isolated carbonate platform in the Western Indian Ocean (Fig. 1A). It extends from the Seychelles (4°S) to Mauritius (20°S), and with an area of 104 510 km² is the second largest carbonate platform of the world. Nine banks form the Plateau, with the Saya de Malha Bank being the largest (Vecsei, 2000; Vortsepneva, 2008). The seafloor morphology in the study area has been mapped previously during fishery research activities (Fedorov *et al.*, 1980; Vortsepneva, 2008), describing a shallow submerged ring reef (at about 40 m water depth) open to the south, a shallow lagoon (40 to 100 m), a deep lagoon (100 to 200 m), a limestone plateau towards the south, and steep outer slopes. Sampling focused on the biological inventory with trawling and dredging.

Deep Sea Drilling Project, Ocean Drilling Program, and industry wells drilled and recovered the basement and sediment sequences of the Mascarene Plateau. The Seychelles Bank rests on Precambrian granite, and the area between Saya de Malha Bank and Mauritius has a Palaeocene basalt basement originating from the Réunion Hotspot (Meyerhoff & Kamen-Kaye, 1981; Duncan & Hargraves, 1990). Two wells reached the volcanic basement of Saya de Malha Bank and the Nazareth Bank, and K-Ar dates assign it to the Late Oligocene to Middle Miocene. In total 2432 m thick carbonate deposits (deep-water ooze, shallow-marine carbonates and reef carbonates) characterize the succession (Meyerhoff & Kamen-Kaye, 1981).

Three seismic stratigraphic packages overlie the Saya de Malha Bank basement (Betzler *et al.*, 2021), recording a turnover from an atoll-like carbonate platform to the present-day configuration. No exact age assignment could be proposed for this change, but it likely occurred during the Pliocene. The turnover occurs as a platform-wide unconformity which crops out as a hardground at the seafloor in the southern Saya de Malha Bank part. The area with this lithified seafloor is located where the South Equatorial Current (SEC) flows with highest velocity (Betzler *et al.*, 2021).

The SEC transports approximately 50 Sv, primarily driven by strong south-east trade winds between 10°S and 30°S. The highest energy of the SEC extends from the sea surface down to 300 m water depth (Feng & Wijffels, 2002). Mean flow to the west over the sill separating Saya de Malha Bank and Nazareth Bank is 50 to

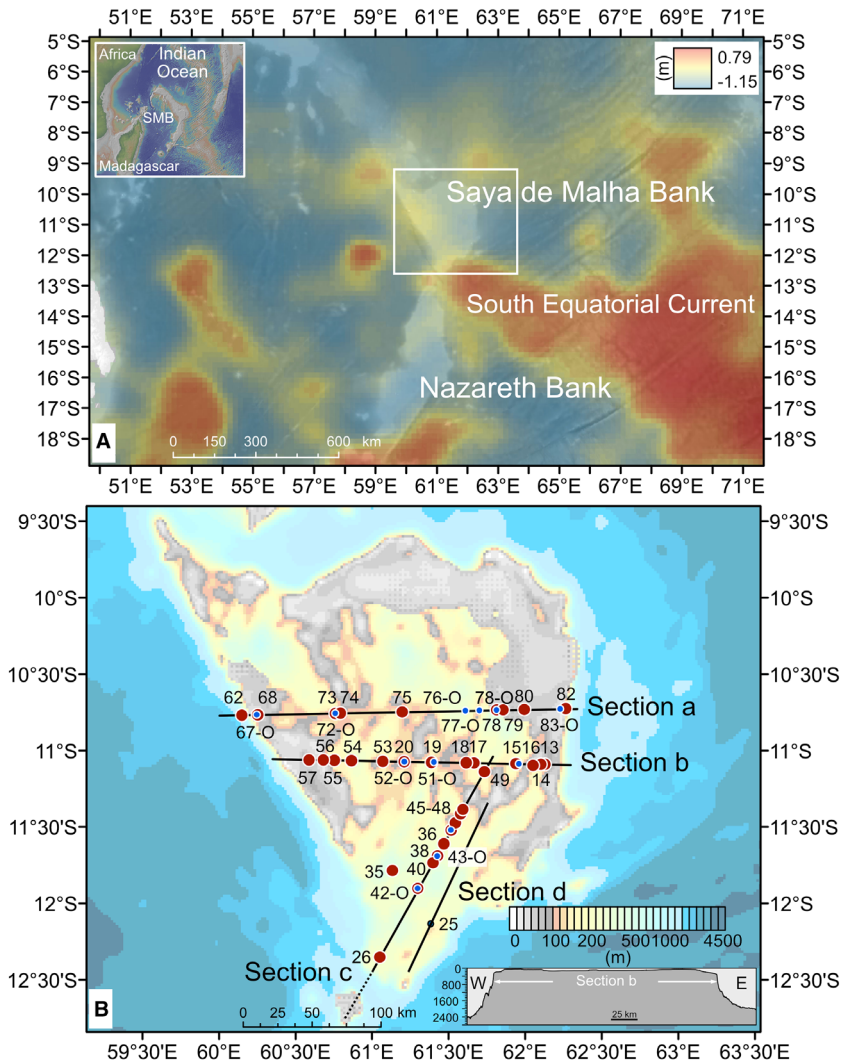


Fig. 1. (A) Location of the Saya de Malha Bank in the central Indian Ocean with sea-surface elevation. Higher elevations are in zones of higher current velocities. The South Equatorial Current (SEC) around 12°S with its highest velocities encounters the southern tip of Saya de Malha Bank (SMB). (B) Saya de Malha bank with analysed samples (red dots), Ocean Floor Observation System (OFOS) data (blue dots), conductivity, temperature and depth (CTD) station 25 as well as positions of Sections a to d. Stippled part of Section c includes the prolongation of the section shown in the ADCP data (Fig. 9A and B). The inlay shows a cross-section (based on SO270 cruise multibeam data) along Section b.

70 cm s⁻¹ fast (New *et al.*, 2007). In the upper, well-mixed layer (50 to 100 m), the currents are more or less uniform and weaken downward to 500 to 1000 m. At Saya de Malha Bank barotropic tidal currents with both semi-diurnal and diurnal constituents can add 35 cms⁻¹ in the east–west direction during spring tides.

At the sill separating Saya de Malha Bank and Nazareth Bank, two types of tidal internal waves are generated (Konyaev *et al.*, 1995; da Silva *et al.*, 2011, 2015; New *et al.*, 2013). One type of IW forms at a density front at the eastern crest, upstream of the sill and propagates with a speed of 2.57 m s⁻¹ (da Silva *et al.*, 2015). The other IWs are triggered at a depression of the deepest isopycnal down to 100 m of water depth, leeward of the sill and move at a speed of 0.65 m s⁻¹ (da Silva *et al.*, 2015). The IWs

propagate onto the southern part of the Saya de Malha Bank (Fig. 2; New *et al.*, 2013) and have not been traced further into the platform in areas shallower than approximately 150 m (Fig. 2).

The annual sea surface temperatures on Saya de Malha Bank range between 24°C and 28°C. In spite of the position of the bank in the SEC water flow, there is no topographic upwelling of nutrient-rich waters into the euphotic zone (Betzler *et al.*, 2021). This is reflected by low phosphate and chlorophyll-alpha concentrations in the waters over the bank.

METHODS

High-resolution subsurface data were acquired with the ship-based parametric sediment echo

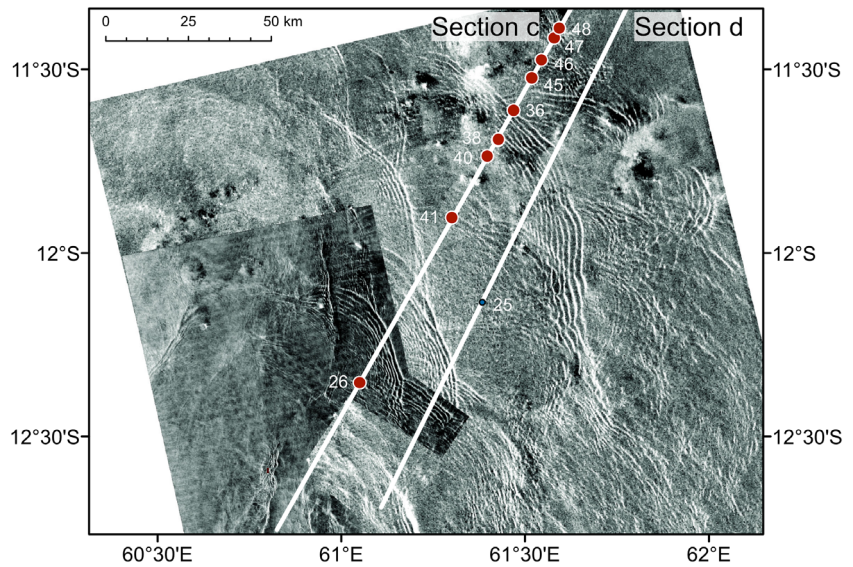


Fig. 2. Composite synthetic aperture radar (SAR) satellite imagery from 21 March 2011 after New *et al.* (2013) showing the internal waves generated in the passage between Saya de Malha Bank and Nazareth Bank propagating towards the north-east. The white lines indicate the positions of the sections shown in Figs 10 and 11 with location of box cores and CTD Station 25.

sounder (Atlas Parasound, PS70; frequencies set to 19.8 kHz and 4 kHz; Teledyne Marine, Daytona Beach, FL, USA; Lindhorst *et al.*, 2019). Time–depth conversion is based on an average sound velocity in water of 1500 m s^{-1} . Bathymetric information was acquired with the ship-based multibeam (swath echosounder) systems (Kongsberg EM122, EM710; Kongsberg Maritime, Kongsberg, Norway).

Current measurements were done using the 38 kHz shipboard Acoustic Doppler Current Profiler (ADCP) of Teledyne RD Instruments (Lindhorst *et al.*, 2019) and the Teledyne RD Instruments software package VmDas. The ADCP was configured for bottom tracking with 35 bins of 24 m and a blanking distance of 24 m. The first depth cell centre is located at 42.4 m and the lowermost at 816 m of water depth. The ADCP data was post-processed with the CODAS3 Software System (https://currents.soest.hawaii.edu/docs/adcp_doc/).

A 144-channel digital streamer system (Hydroscience Technologies Inc., Mineral Wells, TX, USA; active length 600 m, hydrophone group interval 4.167 m) acquired the reflection seismic data (Lindhorst *et al.*, 2019). A two-airgun array towed on a traverse at 2.5 m water depth behind the ship with a standard and a mini GI gun, configured in true GI mode with a total volume of 150 and 45 cinch (3.2 l), respectively, served as seismic source. The guns were operated at 150 bar at a survey speed of 5 to 5.5 kn. A distance-controlled trigger was applied at a 21 m interval. Data were processed with a

Halliburton-Landmark ProMAX® 2D software package and a pre-stack normal dip moveout was applied. Data were stacked with a bin size distance of 8.4 m resulting in an average CDP fold of 66. Ocean seismics processing included the attenuation of the direct water wave, gain recovery, source signature deconvolution and amplitude calibration. For direct wave attenuation an eigenvector filtering was applied. To maintain a ‘true’ amplitude reflection response of the reflectors in the water column, a source signature deconvolution was applied for each shot-gather to account for the source components of the source wavelet. Stacking was utilized with a constant velocity of 1500 m s^{-1} for NMO correction.

Sediment composition and facies assignment integrate sampling with a box corer and visual seafloor observation. The box corer recovered sediment-surface samples of an area of 200 cm^2 with a maximum penetration depth of 45 to 46 cm. Bulk samples of the upper 5 cm of the box cores were wet sieved ($>2 \text{ mm}$; 2.0 to 0.5 mm; 0.5 to 0.250 mm; 0.25 to 0.063 mm; and $<0.063 \text{ mm}$). The samples of the fractions $>2 \text{ mm}$; and 2.0 to 0.5 mm were analysed with a binocular microscope and components were classified according to their abundances in: present (1 to 2%), rare (2 to 5%), abundant (5 to 10%), very abundant (10 to 24%) and dominant ($>24\%$). To identify small-sized bioclasts, thin sections were made. To preserve the texture of the unconsolidated sediment the samples were freeze dried and solidified in vacuum with blue coloured Epoxy resin.

Seafloor images were captured using an Ocean Floor Observation System (OFOS), a video sled with two cameras (video Marshal CV350-5X, and photo Canon EOS 5D Mark IV) and four LED lights pulled at a variable distance from the seafloor. The OFOS has three laser pointers with a permanent distance of 40 cm to determine the scale of the photographs. OFOS position was tracked by a Posidonia USBL positioning system (Lindhorst *et al.*, 2019).

X-ray diffraction analyses were performed at the University of Haifa, Israel, to determine the relative wt% of aragonite, low-magnesium and high-magnesium calcite. Measurements were made on fine fraction samples (<0.063 mm). Calibration curves of the integrated peak area or peak height were used to determine the mineral percentages. Due to a high calcite content, the integrated peak area was used. Depending on the different diffraction angles of carbonate minerals the wt% abundances can be detected (Petschick, 2002).

RESULTS AND INTERPRETATION

Bank-interior morphology

The width of the shallow platform part is 250 km along a northern transect and 160 km along a southern transect (Fig. 3). The western

and the eastern parts of the platform have up to 40 km wide elevated flat-topped rims reaching a water depth of 20 m. The eastern rims are wider than the western ones. Towards the inner part of Saya de Malha Bank, the seafloor deepens to a water depth of around 130 m, and the slope of the eastern rims is gentler than those in the west, which are stepped. In the Saya de Malha Bank interior, several up to 20 km wide isolated highs occur with tops 80 to 100 m deep. The north-east/south-west oriented profile resembles a distally steepened ramp morphology with a minimum water depth of 80 m. The seafloor steepens down to *ca* 300 m water depth at a knickpoint at 120 m water depth. At 300 m, the relief flattens out and shows a 60 km wide and *ca* 50 m high bulge.

Sediment composition

Five sedimentary facies were identified on Saya de Malha Bank: Coralgal facies, rhodolith facies, foraminifera–pteropod sand facies, bioclastic sand facies and hardgrounds (Fig. 3). Detailed semiquantitative compositional descriptions are provided in Supplements S1 to S6.

Coralgal Facies

The Coralgal Facies occurs in the shallow-water areas of the eastern bank margin where the occurrence of live corals is restricted to water

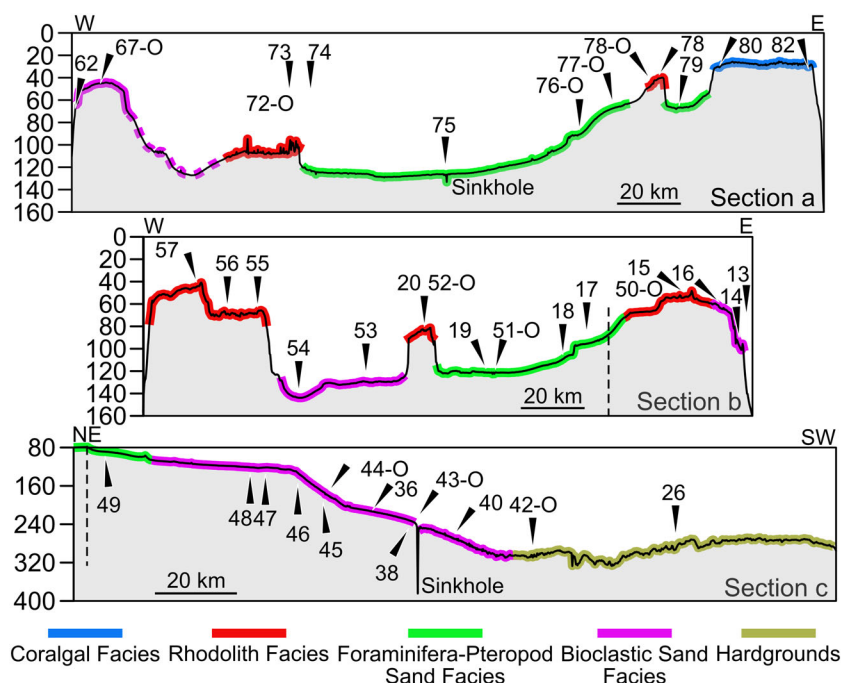


Fig. 3. Cross-sections through the Saya de Malha Bank based on multibeam bathymetry with distribution of facies described in the text. Location of sections shown in Fig. 1B. Numbers indicate position of box core samples, numbers with the extension -O indicates location of OFOS (Ocean Floor Observation System) surveys. Stippled lines indicate intersection of sections b and c.

depths between 20 m and 30 m. In general, corals are not abundant, and between 25 m and 30 m water depth the coral cover is less than 20%. In deeper waters, the corals are replaced by the green algae *Halimeda*. In between the corals and *Halimeda*, rhodoliths are abundant at the sediment surface.

In detail, the facies was observed at stations 78-O, 80 and 83-O (Fig. 4) in water depths of 37 m, 22 m and 31 m, respectively. At station 78-O, corals, together with rhodoliths, *Halimeda* and sea grass characterize the seafloor. Additionally, sea urchins and sea cucumbers were observed. The seafloor at station 83-O is covered by living encrusting corals up to 40 cm wide and branching corals up to 20 cm wide. Coral bleaching has not been registered. The very abundant rhodoliths, up to 9 cm in size occupy >60% of the surface. They are irregular to ellipsoidal in shape, which is conditioned by bioclastic nuclei, some of them coral fragments. Around the nucleus, the rhodoliths are made up of thin, laminar encrusting and warty, rarely fruticose, thalli of coralline algae and peyssonneliaceans (aragonitic red algae), intergrown with bryozoans and encrusting foraminifera. Coralline

algae belong to the order Hapalidiales, mainly to the genus *Lithothamnion*. Other frequent elements are sponges and green algae (*Halimeda* and fleshy), some of them anchored on rhodoliths. Dead corals are present, some up to 1 m wide, minor corals with white disease were found. At station 83-O, the OFOS transect covered water depths between 31 m and 43 m. In the deeper part, the seafloor is mostly covered by green fleshy algae, sporadic coral colonies and few rhodoliths. Sediment at Station 83-O is further rich in larger benthic foraminifera (LBF).

The poorly sorted matrix of the sediment of this facies has a mean grain size of 1.5 mm. It contains abundant *Halimeda* fragments and LBF (*Heterostegina*, *Amphisorus*, *Operculina* and *Amphistegina*) with a moderate preservation. Aragonite is the dominant carbonate mineral with a mean of 46%. High-magnesium calcite and low-magnesium calcite (HMC and LMC) contents are 40% and 14%, respectively.

Rhodolith Facies

On terraces and on seafloor elevations in the interior of Saya de Malha Bank at water depths below 45 m corals or *Halimeda* are absent. The

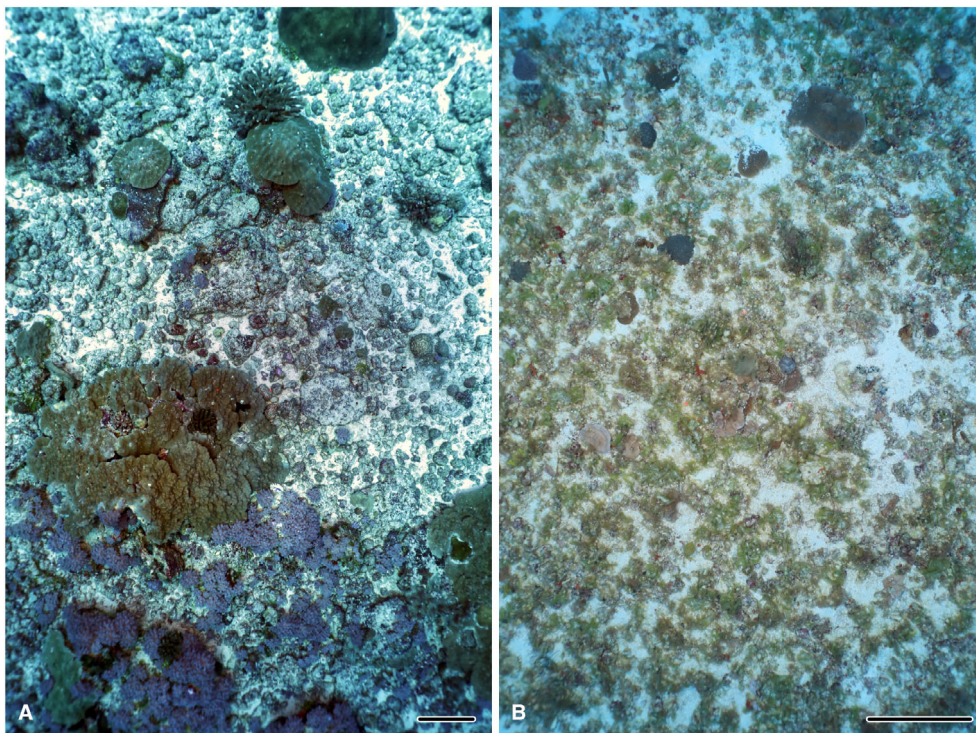


Fig. 4. Ocean Floor Observation System (OFOS) photographs of the seafloor at station 83-O (Coralgal Facies) in a water depth of 31 m (A) and 43 m (B). Lengths of scale bars: 40 cm.

Rhodolith Facies occurs down to water depths of 100 m. This facies is registered at stations 15, 16, 20, 50-O, 52-O, 57 and 73 (Figs 3 and 5). At stations 50-O and 52-O, the surface cover of

living rhodoliths varies between 43% and 8%. The rhodoliths are not evenly distributed at the seafloor (Fig. 5A to C). Locally they are concentrated in the troughs of ripples (Fig. 5A) with

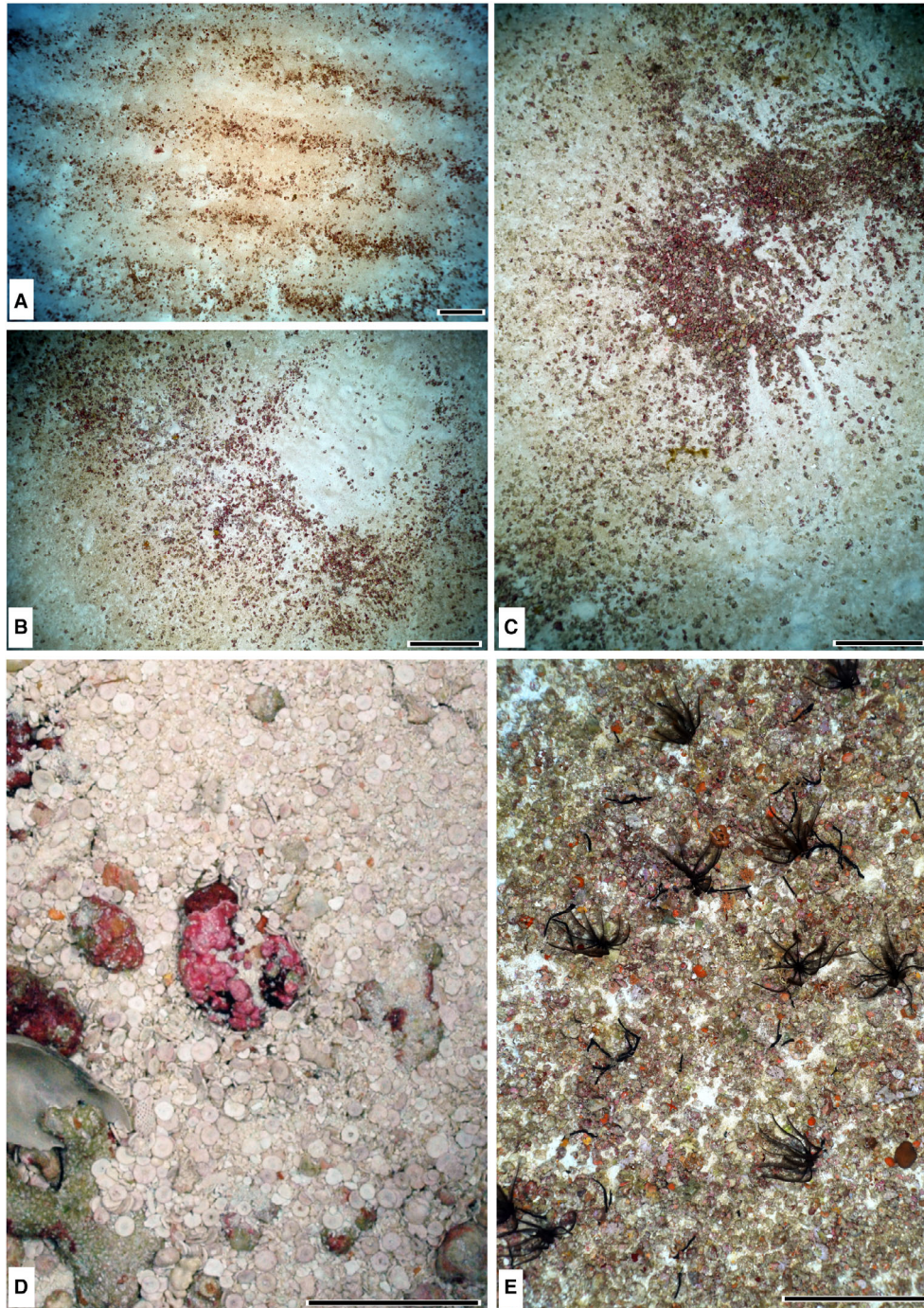


Fig. 5. Ocean Floor Observation System (OFOS) photographs of the Rhodolith Facies. (A) Rippled seafloor at station 50-O in a water depth of 50 m with rhodoliths mostly enriched in the ripple troughs. (B) Rhodoliths at station 52-O in a water depth of 80 m. (C) Rhodoliths at station 52-O. (D) Sediment surface in a box core from station 52-O rich in the large benthic foraminifera *Marginopora*. (E) Rhodoliths and crinoids at station 50. Scale bars A–C, E: 40 cm; D: 5 cm.

wavelengths of 20 to 30 cm. Rhodoliths are also arranged in patches with diameters of up to 110 cm (Fig. 5B and C). Rhodolith patches and almost rhodolith-free areas at the seafloor are located side by side, with relatively sharp boundaries. In some cases, the patches are surrounded by radial ridges enriched in rhodoliths (Fig. 5C). Where ripples are present at the seafloor, a mat-like greenish cover also occurs. Ripples are interrupted by small mounds of whitish sand formed by bioturbation (Fig. 4A). Sea urchins are locally abundant. At stations 15 and 16, the majority of rhodoliths are open-branching, fruticose nodules (maêrl), up to 3 cm in size, made up of a monospecific Hapalidialean. Irregular and spheroidal rhodoliths, less than 3 cm in size, formed by thin laminar encrusting to warty Hapalidiales, scarce Sporolithales and Peyssonneliaceans occur in lesser proportions. This latter type of rhodolith, up to 6 cm but generally less than 2 cm in size, predominates the remaining sampling stations of this facies.

The sediment between rhodoliths consists of coarse sand (Fig. 5D) and contains LBF such as *Amphistegina*, *Heterostegina*, *Amphisorus*, *Operculina* and *Borelis*, as well as molluscs. In general, the preservation of the components ranges between very good and moderate. The main carbonate mineral is HMC with an average value of 47%. Aragonite and LMC make up 27% and 26% of the carbonate fraction, respectively.

At station 50-O, which is located on the eastern elevated shoulder of Saya de Malha Bank (Fig. 3), in a water depth of 50 m, rhodoliths are associated with crinoids (Fig. 5E). There, the rhodoliths form a dense and almost complete cover with only minor patches of carbonate sand scattered at the seafloor.

Foraminifera–Pteropod Sand Facies

This facies occupies the interior of Saya de Malha Bank at water depths between 75 m and 130 m at stations 17 to 19, 49, 51-O, 74 to 77-O and 79 (Fig. 3). Sediment structures comprise ripples and burrows (Fig. 6), some of them up to 20 cm wide (conical mounds). Ripples locally develop a honeycomb pattern with interfering ripple crests. At places, patches of lithified surfaces appear at the seafloor, which are populated by soft corals (Fig. 6A). Locally, the sediment surface is populated by very abundant brittle stars (Fig. 6B). A mean grain size of 0.078 mm defines the well-sorted, very fine sand of this facies. Abundant pteropod tests and planktonic foraminifera, as well as molluscs with a good to

moderate preservation mark the sediment fraction coarser than 0.5 mm, and *Operculina* represents the LBF in this facies. Aragonite and HMC are the main carbonate minerals with an average of 38% and 35%, respectively. Low-magnesium calcite values are at 27%.

The foraminifera–pteropod sands extend in the central depression of Saya de Malha Bank between isolated banks and the Saya de Malha Bank marginal highs. Hydroacoustic data image a well-stratified succession which overlies the elevated areas (Fig. 6C). Reflections are parallel to sub-parallel with some areas of inclined layering. U-shaped to V-shaped depressions cross-cut the sediments, and are interpreted as infilled karst sinkholes. At the seafloor and in the subsurface at a water depth between 120 m and 121 m, there are some bodies with an irregular top and an irregular internal layering (Fig. 6C). Given the water depth at which these structures are located today, it is proposed that they are reef bodies which formed during the last sea-level lowstand.

Bioclastic Sand Facies

Bioclastic sands occupy a variety of locations in the interior and the edges of Saya de Malha Bank in varying water depths. At stations 53, 54, 62, 67-O and 68, at water depths between 30 m and 120 m, the bioclastic sands are arranged in ripples with a maximum wavelength of 23 cm (Fig. 7A). Rhodoliths appear in ripple troughs covering less than 1% of the sediment surface, and patches of lithified sediment with a cover of tunicates, corals and sponges occur throughout this facies. The bioclastic sands contain planktonic foraminifera, pteropod tests, *Halimeda* fragments, molluscs, coralline red algae and LBF (*Amphistegina*, *Heterostegina* and *Operculina*; Fig. 7B). Low-magnesium calcite and HMC are the main carbonate minerals with 39% and 33%, respectively, and 28% aragonite. The mean grain size of the poorly sorted sand is 0.3 mm, the bioclasts are abraded and fragmented (Fig. 7B).

At stations 13 and 14 and 46 to 48, i.e. at water depths >80 to 160 m, bioclastic sands are moderately sorted with an average grain size of 0.2 mm. They are composed of planktonic foraminifera, pteropod tests, molluscs, coralline red algae, LBF (*Operculina* and *Heterostegina*) with a moderate to poor preservation, and coral fragments. Coralline algae occur in nodules, irregular to ellipsoidal, with shapes strongly conditioned by the bioclastic nuclei and

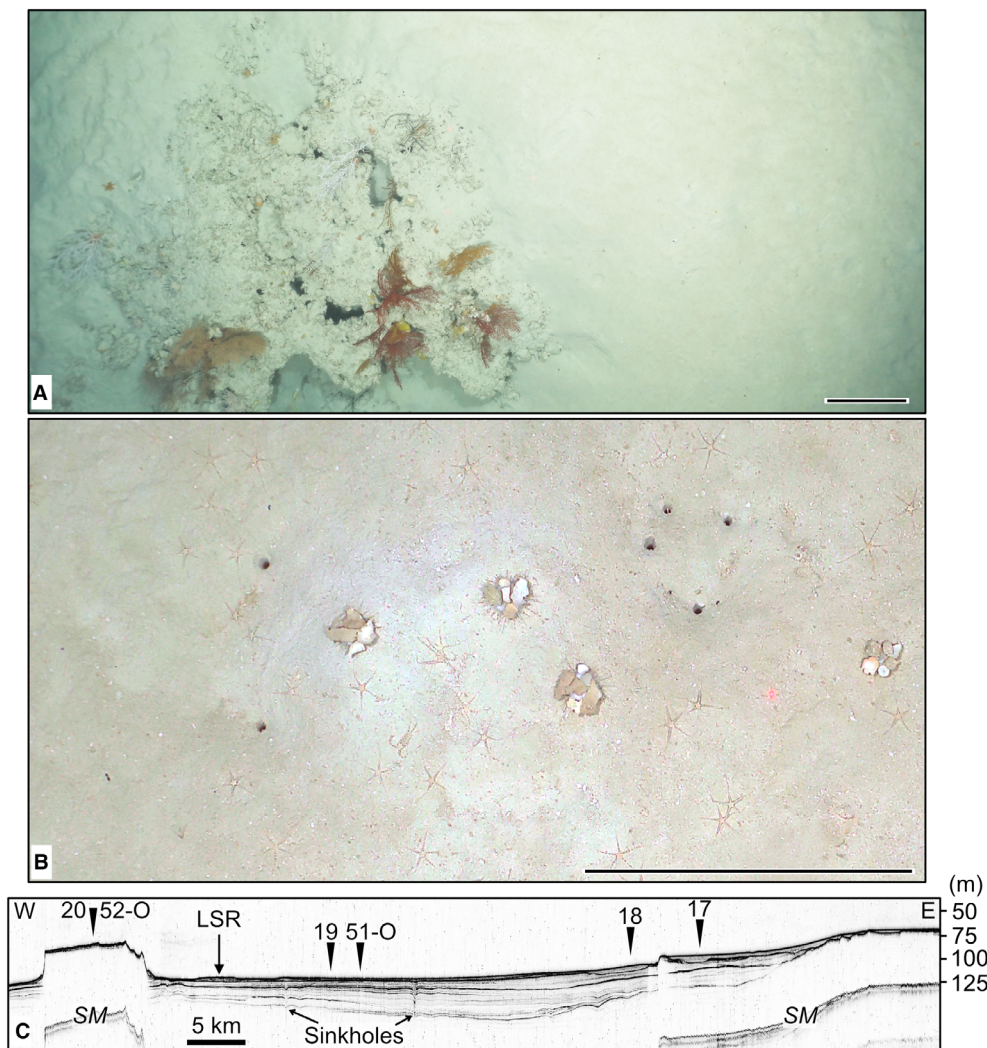


Fig. 6. Foraminifera–Pteropod Sand Facies. (A) Seafloor photograph at station 51-O with rippled sand partially covering a patch of lithified sediment populated by soft corals. (B) Seafloor photograph at station 72-O with abundant brittle stars and echinoids (with shell debris cover). (C) Parasound section of the Saya de Malha Bank (SMB)-interior basin. The foraminifera–pteropod sands are arranged in a well-layered succession between the bank-interior highs. LSR: Lowstand reefs; SM: seafloor multiple.

relatively small sizes (up to 6 cm but generally less than 2 cm). The nodules consist of thin laminar, encrusting to warty thalli of Hapalidaleans. Aragonite is the dominant carbonate phase with 43% followed by HMC with 32% and LMC with 25%.

Towards the southern part of Saya de Malha Bank at stations 36, 38, 40 and 53, at water depths down to 200 m, bioclastic sands are poorly sorted with a mean grain size of 0.3 mm. Pelagic organisms (pteropods and planktonic foraminifera), molluscs, bryozoans and coralline red algae are the most common components. These sediments form ripples and asymmetrical

megaripples. The pelagic organisms exhibit good preservation while the rest of the components are poorly preserved. Low-magnesium calcite and aragonite are the main carbonate minerals both with 36%, and HMC with 28%. Cemented patches are locally present.

At the deepest station located in the interior of Saya de Malha Bank (>160 m, stations 44 and 45) the bioclastic sands form ripples and megaripples, which partially cover the seafloor (Fig. 7C). Coarse materials, such as shell debris, rhodoliths and corals occur in the troughs. The megaripples have a height of 2 m and a wavelength of around 100 m. A mean grain size of

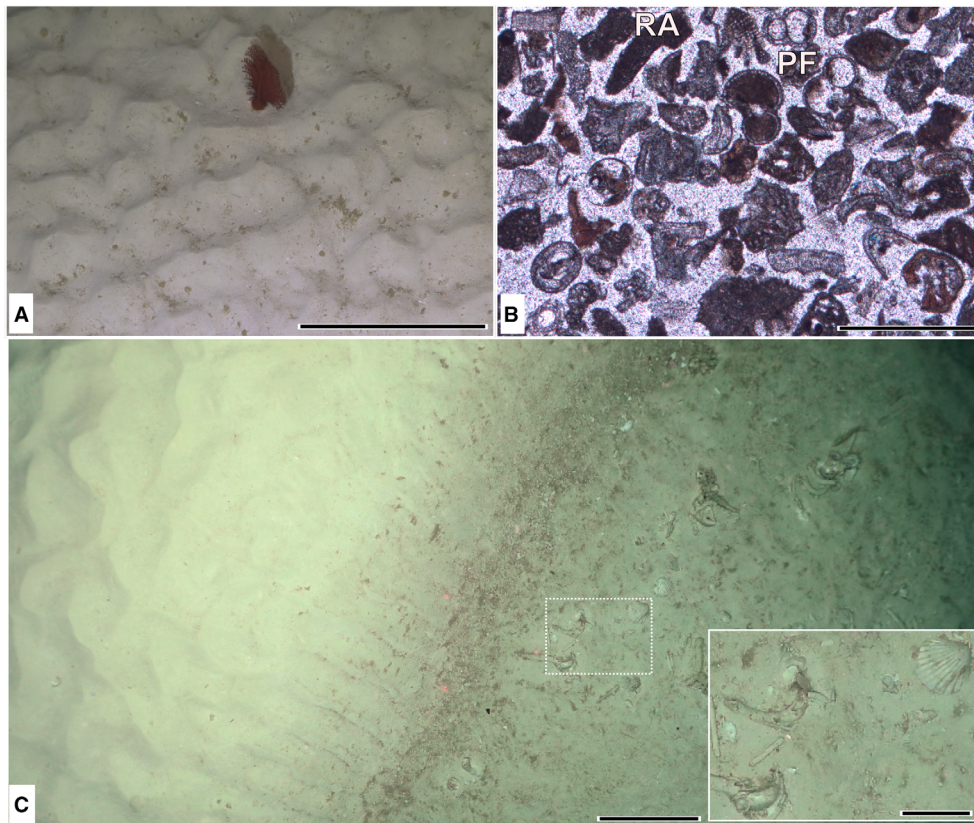


Fig. 7. South Equatorial Current Bioclastic Sand Facies. (A) Ocean Floor Observation System (OFOS) image of the seafloor at station 36-O with linguid ripples and sea pen. (B) Thin section photograph of unconsolidated bioclastic sand with diverse abraded bioclasts and planktonic foraminifera (station 36). RA: Red algae; PF: Planktonic foraminifera. (C) Seafloor image of the bioclastic sands at station 44-O. The crest and the flanks of the megaripple are covered by linguid and straight-crested ripples. The trough of the megaripple is covered by coarse-grained bioclasts (for example, *Pecten* in the amplified view, location of this view indicated by stipple-lined rectangle) and exhumed tubular lithified burrows. Scales: A, C: 40 cm; amplified view: 10 cm. B: 5 mm.

0.5 mm characterizes the sediment. Components >0.5 mm are dominated by pelagic organisms (planktonic foraminifera and pteropod tests) with a good preservation. Other components are molluscs, coralline red algae and LBF (*Amphistegina*) with a moderate to poor preservation.

Hardground

A hardground as a laterally extensive surface occurs at water depths >300 m at the southern end of the Saya de Malha Bank (stations 26 and 42-O; Fig. 3). The lithified seafloor is colonized by ophiuroids, crinoids and black cold-water corals (*Antipatharia*; Fig. 8A). The hardground has a brownish colour and is dissected by irregular fractures (Fig. 8B). Locally, the hardground is covered by patches of submarine dunes consisting of bioclastic sand waves with a height of up to 7 m and wavelengths up to 233 m (Fig. 8C and D).

Ocean currents and internal waves

Acoustic doppler current profiler data

Figure 9A and B show the current velocity distribution at the southern tip of Saya de Malha Bank along Section c. The record encompasses a 23-h transect along a north-east – south-west traverse. The section crosses from the trough between Nazareth Bank and Saya de Malha Bank into the shallow part of Saya de Malha Bank. In the trough, below 150 m the flow is directed to the north-west – west and corresponds to the flow direction of the SEC. The surface near layer of the trough, as well of the bank area north-west of it, shows strong west to south-west currents. On the shallowest part of the bank, the currents are also strong and directed west to south-west. In the middle part of the bank the currents are less pronounced. Highest

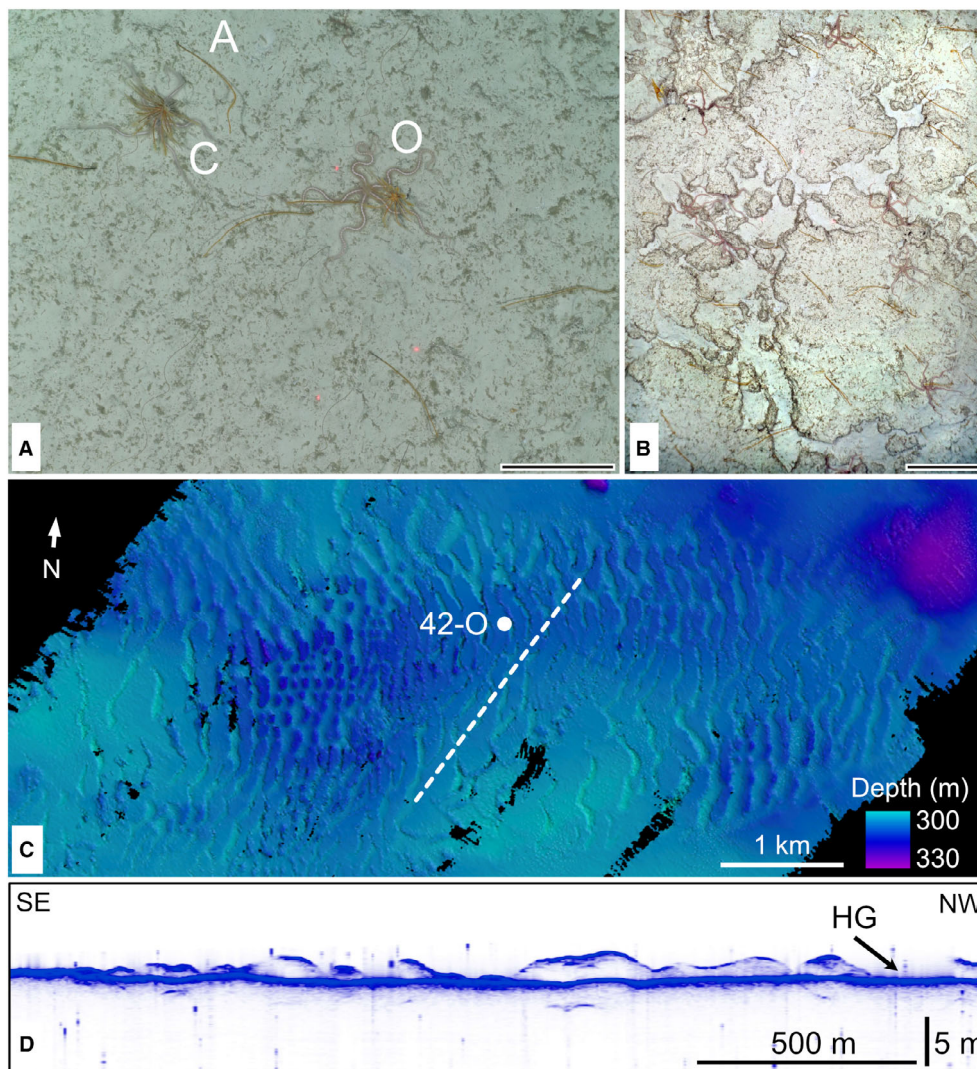


Fig. 8. Hardground. (A) Ocean Floor Observation System (OFOS) seafloor image at station 42-O shows a lithified surface with poor sediment cover and ophiuroids ('O'), crinoids ('C') and Antipatharia ('A'). (B) Seafloor image of a hardground dissected by irregular fissures (station 22-O). (C) Multibeam map of the seafloor around station 22-O with the hardground covered by submarine dunes. Black areas: data gaps. The stippled line indicates the position of the Parasound section in (D). (D) Parasound profile showing the thin and irregular sediment cover above the hardground (HG).

current velocities reach values of up to $\pm 100 \text{ cm s}^{-1}$.

Figure 9C to E show the evolution over time of the velocity components and the received signal strength at station 25. The ship stayed at this position for 20 h and 35 min. The sampled ADCP data were averaged over a period of 5 min. The distance travelled by the vessel during the collection period was negligible (215 m). During the first 5 h on station and from hour 12 to 19 the current flow has a dominant west-directed component with velocities of up to

80 cm s^{-1} . The time interval between 5 h and 12 h is marked by weaker currents which are rather directed towards the south-east – north-east.

In the ADCP signal strength, which depends on the concentration of suspended particles, there are two kinds of signal domains, each displaying vertical fluctuations of the depth position of reflectivity layers in the water column. From 00:00 to 02:30 hours and 08:30 to 14:00 hours the water column stratification fluctuated with smooth amplitude heights (about

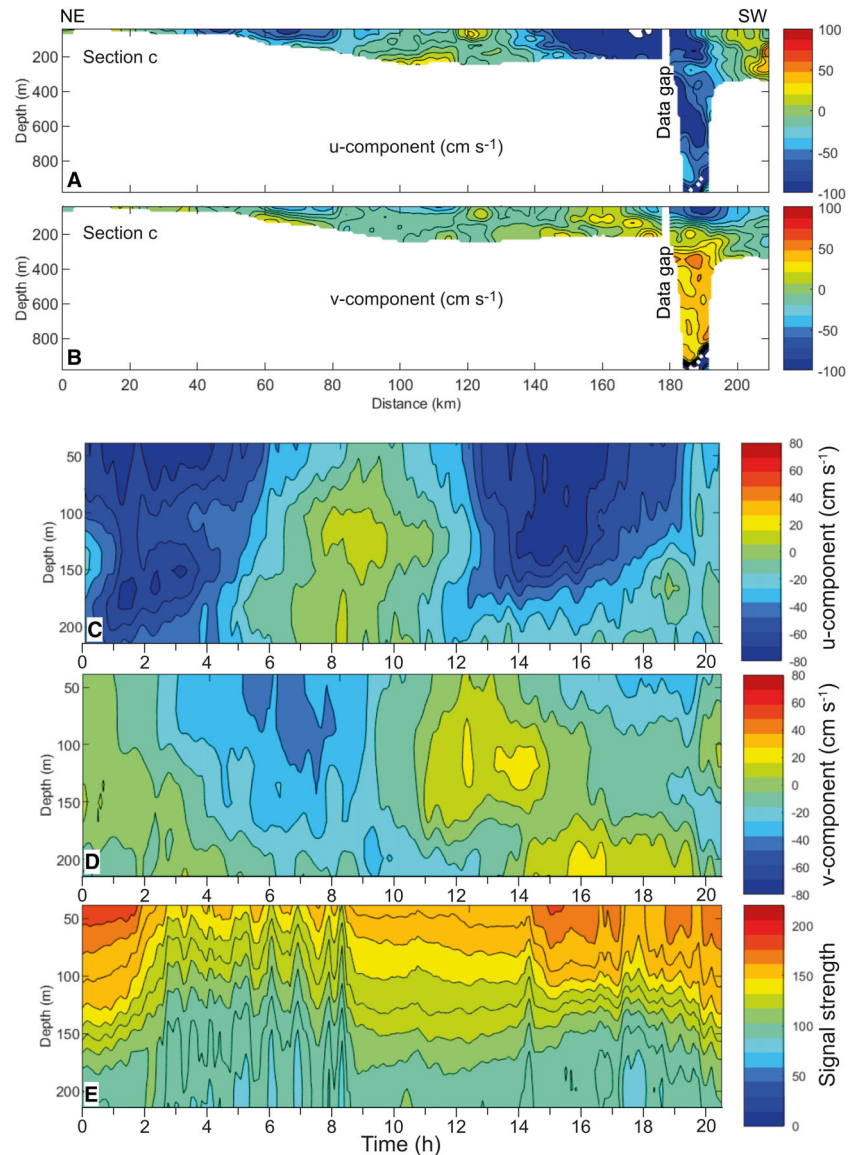


Fig. 9. (A) East – west current velocity as measured with ADCP. The west-directed South Equatorial Current (SEC) flows with a speed of up to 1 m s^{-1} through the passage between Saya de Malha Bank (SMB) and Nazareth Bank and over the southern tip of SMB. (B) South – north current velocity as measured with ADCP. Location of Section c shown in Fig. 1. (C) and (D) Hovmöller diagram of velocity (C: east–west component of velocity; D: north–south component of velocity) and signal strength of 38 kHz ADCP (E) at station 25 ($13^{\circ}51.9'S$, $61^{\circ}23'E$).

10 m) and a period of about 40 min. In the intervals between 02:30 and 08:40 hours and starting at 14:00 hours, the fluctuations are dominated by much larger amplitudes (about 30 m) and periods of about 60 min. These variations were better defined in the earlier time interval.

The ADCP data from Saya de Malha Bank are interpreted to reflect the influence of the internal tides and related internal waves on the current regime (da Silva *et al.*, 2011, 2015; New *et al.*, 2013). The long-term variations in current speed and current direction (Fig. 9C and D) are interpreted to reflect the internal tide impinging on the southern Saya de Malha Bank with amplification and attenuation of the South Equatorial Current velocity during rising and falling

tides. Highest current velocities occur during falling tides. Both wave types, internal tides and related internal waves are imaged in the backscatter signal strength variations (Fig. 9E) with the shorter periodicity fluctuations as a consequence of the internal waves and the long-term variations reflecting the internal tides.

Ocean seismic and Parasound data

The internal waves are also visible in seismic imaging of the water column (Fig. 10). Along Section c (Fig. 10A) the upper part of the water column in the ocean seismics appears transparent, with a first reflection at the base of this interval at *ca* 120 ms TWT. This first reflection coincides with the top of the thermocline. The

depth level of this reflection changes from *ca* 90 m to 130 m depth in a wave-like pattern along the seismic lines, which means during the recorded interval of time.

Reflection depth changes show two distinct patterns. Higher amplitude lowering of the thermocline of *ca* 100 ms TWT (*ca* 75 m) have an apparent duration of around 1 to 1.5 h (Fig. 10A). These lows are accompanied by lower amplitude and shorter term wave-like fluctuations with an amplitude of *ca* 25 m and an apparent period of 8 min (Fig. 10A). Periods and durations are given here as apparent time on purpose, because the exact ship speed (5 kn in average during acquisition of seismic data) and direction of ship track during recording time was not considered in the processing of the ocean seismics. The waves covering the longer time interval are interpreted as internal tides, the waves with a shorter wavelength as the internal waves triggered by these internal tides. Internal tides and internal waves break at a water depth of *ca* 150 m at the knickpoint of the distally steepened ramp (Fig. 10A). A series of box core stations (Fig. 10B and C) allows a compositional and sedimentological characterization of these deposits. Whereas planktonic foraminifera, pteropods, molluscs, echinoids, bryozoans and coral debris occur in all samples of the transect, red algae, *Halimeda* and LBF (*Heterostegina*, *Amphisorus*, *Borelis* and *Amphistegina*) are most common just above the wave base of the internal tides and internal waves.

A nepheloid layer develops downslope in the water column (Fig. 10C), which appears to creep near to the sediment surface before dissipating. Sediment along this transect is coarsest where the internal-wave trains touch ground, and becomes finer grained bankward and basinward (Fig. 10D). The segment with coarser grain size coincides with the part of the transect that is richer in LBF and calcareous algae.

In Fig. 11 the seismics and ocean seismics of Section d are shown (see Figs 1 and 2 for location). As in Section c, the multi-channel high-resolution seismic reflection data of the water column image fluctuations through time. In Fig. 11A, the south-west – north-east running line covers a distance of *ca* 78 km over a time of *ca* 9.1 h. As in Section c, the internal tidal waves and the internal waves break at the seafloor at a water depth of around 150 m, at the break of the slope angle of the distally steepened ramp (Fig. 11A). The water-column image using the Parasound profile shows that the nepheloid

layer develops down-ramp below 150 m depth and fades out towards the south-west (Fig. 11B). Where the wave base touches the sediment surface, there is a 1 km wide and several metre deep trough-like depression. Subsurface data indicate an erosional truncation of strata in this zone. The seafloor in the trough appears as an irregular surface which is related to submarine dunes, up to 4 m high and tens of metres wide (Fig. 11C). Further down-ramp, tabular strata are slightly inclined before changing to a segment with large-scale, low-angle trough cross-beds (100 m wide, 1 to 5 m high). This segment of the distally steepened ramp between 250 m and 300 m of water depth is followed by an area, where the seafloor is covered with large-scale submarine dunes (Fig. 11D) with a wavelength of over 200 m and a height up to 10 m. The remaining part of the ramp displays seaward thinning subparallel strata wedging out over a distance of 20 km (Fig. 11A).

Distribution and crest orientation of the submarine dunes observed in the multibeam data in this part of Saya de Malha Bank are shown in Fig. 12. In the shallowest area covered by submarine dunes (water depth 120 to 140 m) the crests are oriented west – east. In deeper areas, the crests have a north-west – south-east orientation (i.e. Fig. 8C) with a north – south orientation in the deepest zone (water depth >280 m) where such submarine dunes are registered. The apparent direction of migration of the dunes as imaged by foresets is directed south in the deeper areas (Fig. 11D), whereas large-scale low-angle trough cross-beds characterize shallower areas (Fig. 11C).

DISCUSSION

The Saya de Malha Bank is a tropical carbonate platform where reefs do not grow up to sea level. The bank's sedimentary dynamics are therefore especially relevant with regard to questions related to carbonate platform drowning, where the different observed facies are often recorded as a vertical succession. The Saya de Malha Bank is also a natural laboratory to analyse the interaction of ocean currents and internal waves with shallow-water carbonate sedimentation.

Facies distribution

The Saya de Malha Bank is a mesophotic carbonate platform with three distinct sedimentary realms. The shallowest realm is represented by

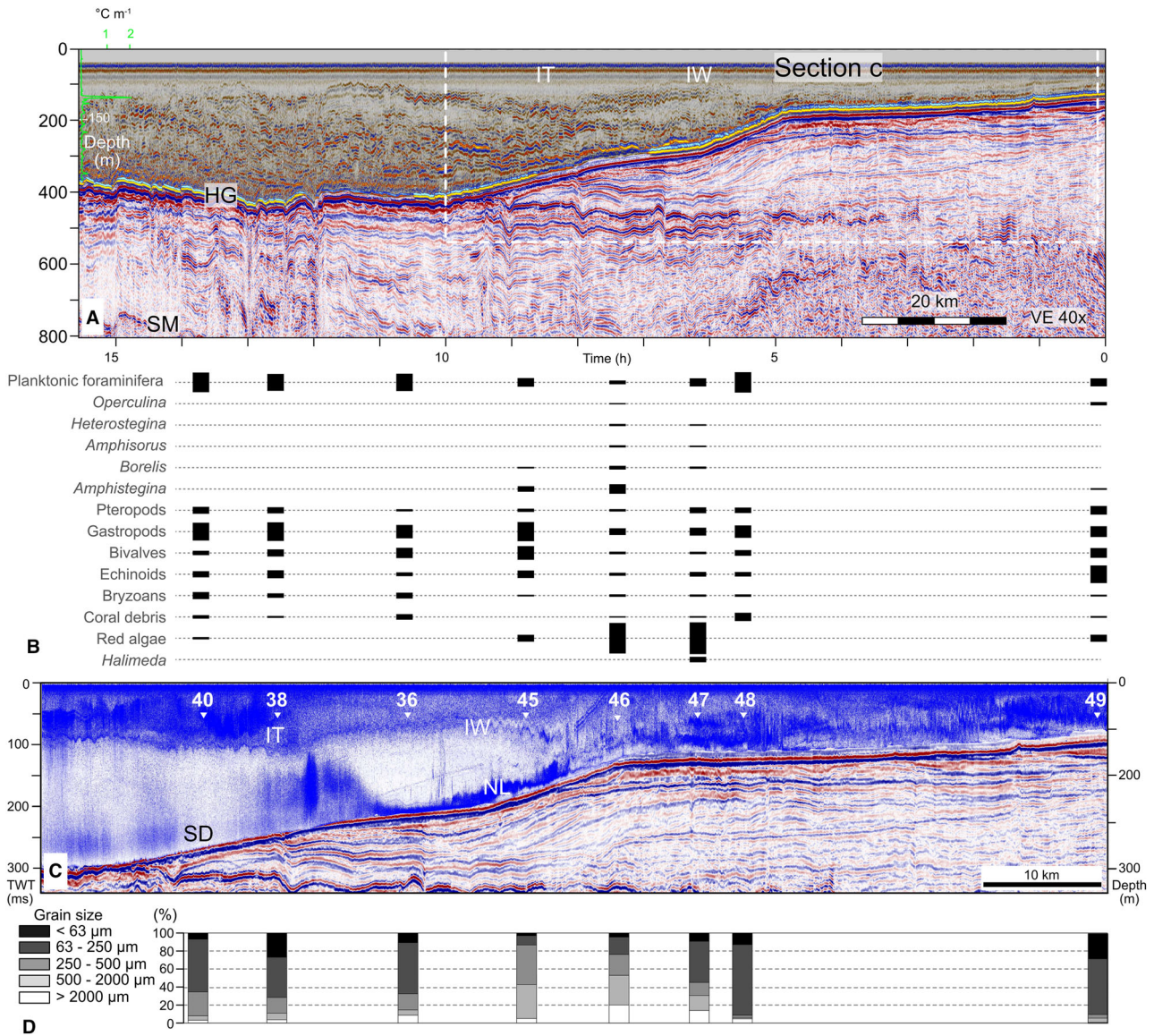


Fig. 10. (A) Composite seismic section (Section c, Fig. 1) with subsurface seismic stratigraphy (lower part) and ocean seismics (upper part). Green curve shows the temperature gradient with depth as measured at a CTD station at 12.69°S and 61.31°E (station outside of the map areas shown in Fig. 1). Long wavelength fluctuations of the water-mass stratification are interpreted to reflect internal tides, the shorter wavelength is interpreted to reflect internal waves (IW). Horizontal scale is given in distance but also in time (ocean seismic data). HG: Hardground; SM: Seafloor multiple. (B) Relative abundance of major components in box core samples along the section (sample location in C; width of rectangles indicates the component abundance). (C) Detail of the transect with subsurface seismic stratigraphy in the lower part and water column Parasound data in the upper part. Internal tides and IW are displayed by moving position of the surface separating abundant suspended components in upper *ca* 100 to 120 m of the water column. Note a nepheloid layer (NL) just above the seafloor below a water depth of *ca* 140 m which appears to mix and dissipate downslope. SD: Submarine dunes. (D) Grain-size variations in the samples along the transect. Note that there is no general fining trend with water depth and that the coarsest sediments are encountered where the base of the internal tides and IW touch ground.

the corallal facies (Fig. 4) and the rhodolith facies (Fig. 5) which represent mesophotic carbonate systems, i.e. areas with active neritic carbonate producers. These facies cover the

seafloor at elevated bank margins and on intra-bank highs (Fig. 3) down to water depths <90 m. The corallal facies is located in waters shallower than the rhodolithic deposits. In the

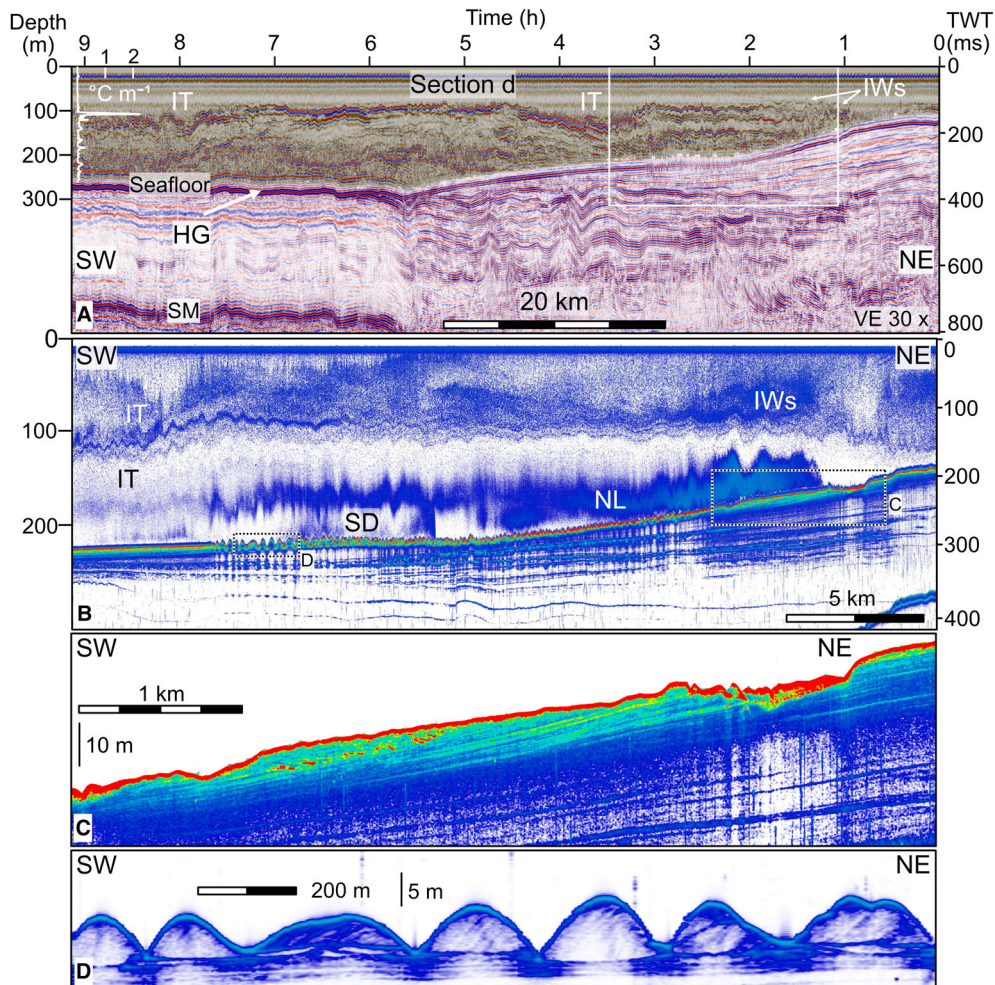


Fig. 11. (A) Composite seismic section (Section d, Fig. 9) with subsurface seismic stratigraphy (lower part) and ocean seismics (upper part). White curve shows the temperature gradient with depth as measured at a CTD station at 12.69°S and 61.31°E (station outside of map areas shown in Fig. 1). Long wavelength fluctuations of water-mass stratification are inferred to reflect internal tides, the shorter wavelength most likely represents internal waves. Horizontal scale is given in distance but also in time (ocean seismic data). HG: Hardground; SM: Seafloor multiple. (B) Detail of the transect with subsurface seismic stratigraphy in the lower part and water column Parasound data in the upper part. Internal tides and IW are displayed by moving position of the surface separating abundant suspended components in upper *ca* 100 to 120 m of the water column. A nepheloid layer (NL) is located just below the internal tide and internal wave base and fades out towards the south-west. SD: Submarine dunes. (C) Erosional scar at the seafloor; submarine dunes are also present. Acoustic properties of the sediment indicated coarser grain sizes than for surrounding sediments (acoustic blanking below the scar). (D) Submarine dunes in the distal part of the transect.

western part of Section a (stations 62 and 67-O; Fig. 3), however, where the seafloor at a depth of *ca* 40 m is covered by bioclastic sand, no neritic carbonate production was registered. This indicates that the facies distribution is not controlled by water depth alone. What other factor is involved, however, cannot be resolved with the available data.

The second realm of the platform is represented by the perched basin in the bank interior,

which is open towards the south (Figs 1 and 3). The perched basin area is occupied by the Foraminifera–Pteropod Sand Facies in the eastern part and by the Bioclastic Sand Facies in the western part (Fig. 3). In Section c, i.e. along a north-east to south-west transect from the platform interior to the outer reaches of the platform, the Foraminifera–Pteropod Sand Facies changes downslope into the Bioclastic Sand Facies. Ripples occur throughout all OFOS

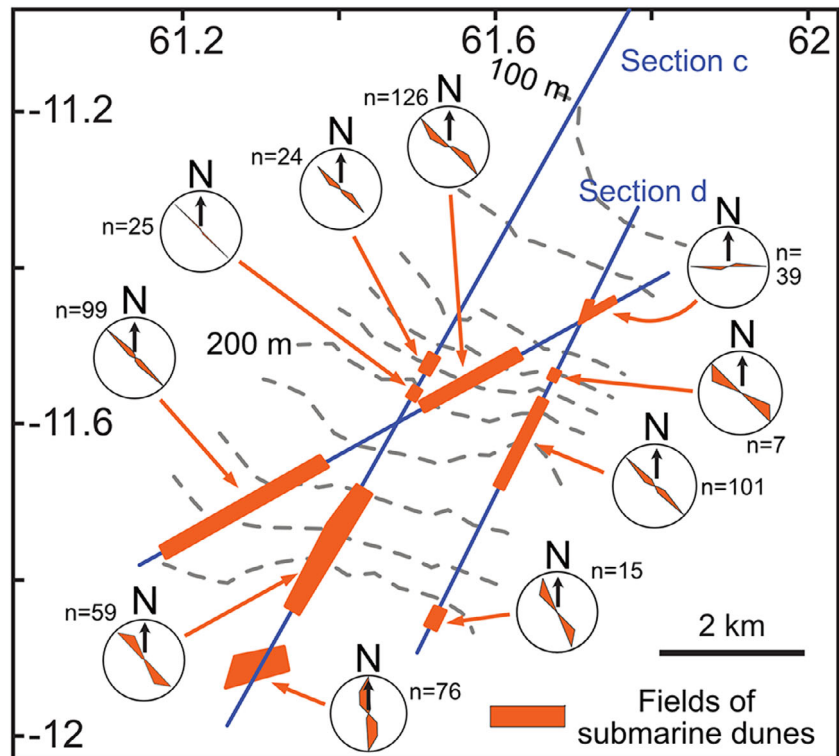


Fig. 12. Areas where submarine dunes were identified in the multibeam and Parasound data (orange) with crest orientations. Blue lines indicate ship tracks. Crest orientation changes from west to east in shallower areas to NNW to SSE in deeper zones. See text for discussion.

stations which indicate bottom current activity in the entire realm. The relief of the seafloor along this transect is that of a distally steepened ramp.

The third realm observed at the Saya de Malha Bank is an area of non-deposition, i.e. the zone represented by the hardground (Fig. 3). It corresponds to the area where the SEC flows over the bank with its highest velocity.

Carbonate-platform drowning

The platform configuration with its lateral facies variations (Fig. 13) combines what is also known from stratigraphic records of carbonate platform drowning, i.e. from the vertical facies superposition which forms during the demise of shallow-water carbonate banks (Zempolich, 1993). Mesophotic reef systems are described as precursor facies to the full demise of shallow water carbonate sedimentation, although they may represent major calcium carbonate factories at depth (Amado-Filho *et al.*, 2012). Mesophotic reefs in most cases are reefs which could not keep up with the post-glacial sea-level rise and are now lying too deep to develop significant growth or accumulation rates (Montaggioni, 2005). In the geological record, mesophotic reefs may form the

intermediate step between the shallow-water facies and the pelagic facies in a drowning sequence. One could conceive that Walther's Law of facies superposition marking a carbonate drowning in the fossil record occurs as a time-equivalent array of facies at SMB.

In the Miocene, the Zhujiang carbonate platform (South China Sea), the carbonate platform overlying the Triton High (Vietnam) and the Yadana carbonate platform (Andaman Sea) all display rhodolith-rich intervals separating the shallow-water reef facies from pelagic marine shales (Erlich *et al.*, 1990; Sattler *et al.*, 2009; Fyhn *et al.*, 2013; Paumard *et al.*, 2017; Strohmenger *et al.*, 2020; Teillet *et al.*, 2020). A similar sequence was described for the Lower Jurassic Jbel Bou Dahar carbonate platform (Morocco) with high-energy deposits and low-diversity assemblage on top of the platform succession, covered by onlapping mudstones (Bloemer & Reijmer, 1999). Current-controlled and hemipelagic bioclastic carbonate sands overlying carbonate platforms were described in Italy (Marino & Santantonio, 2010) and also atop multiple drowned Cretaceous platforms (Wilson *et al.*, 1998; Jenkyns & Wilson, 1999; Bialik *et al.*, 2021). Hardgrounds were described as drowning unconformities (Schlager & Camber, 1986), i.e. a stratigraphic surface witnessing

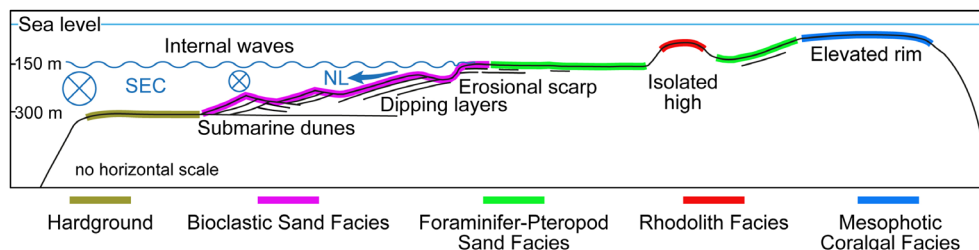


Fig. 13. Conceptual scheme with key sedimentological features and controlling factors on the Saya de Malha Bank. SEC: South Equatorial Current, NL: Nepheloid layer. The section is roughly oriented north-east – south-west.

an interruption or even shutdown of shallow-water carbonate production.

The potential of a tropical shallow-water carbonate factory to infill accommodation has been seen as a function of the interrelation of an increase in the rate of accommodation and carbonate production. The latter traditionally has been linked to controlling factors such as temperature, salinity, nutrients, turbidity and siliciclastic input, all of which were assumed to affect the benthic carbonate or reef growth potential (Kendall & Schlager, 1981; Hallock & Schlager, 1986; Schlager, 1991; Jenkyns & Wilson, 1999; Mutti *et al.*, 2005).

Variations in temperature and salinity can be ruled out in the case of the tropical Saya de Malha Bank lying in the open Indian Ocean; siliciclastic influx and turbidity are also negligible because the platform is an isolated platform. Finally, high nutrients contents in and around the bank were not reported in measurements on and around the platform area discussed herein (Betzler *et al.*, 2021). It has been reported (Rosset *et al.*, 2017) that corals can tolerate an undersupply of nitrogen but that low phosphate contents have negative effects on symbionts eventually resulting in bleaching. The phosphate (PO_4) content in the upper water masses of the Saya de Malha Bank are around or below $0.25 \mu\text{mol kg}^{-1}$ (Betzler *et al.*, 2021). Bleaching has not been registered in the data acquired and therefore the PO_4 values are not seen as a limiting factor of coral growth.

Montaggioni & Martin-Garin (2020) show that sea level was at least 100 m lower than today from 20 000 to 18 000 years BP in the western Indian Ocean. Between 17 000 and 10 000 years BP, shallow-water corals grew in positions now at water depths between 130 m and 50 m. It was inferred that the modern western Indian Ocean reefs, which reach sea level today, began

growing *ca* 9600 years ago with a 20 m lower sea level. These reefs would have had a growth rate of 1 to 10 mm year^{-1} , which is much lower compared to the early Holocene sea-level rise rate of up to 19 mm year^{-1} in the western Indian Ocean (Zinke *et al.*, 2005). Given that production rates of modern reefs are mostly light-dependent (Bosscher & Schlager, 1992) these mesophotic reefs are now too deep to develop high enough accumulation rates to infill Holocene accommodation. Anthropogenic climate change is expected to result in rapid sea-level rise of up to 3 m by the year 2200 (DeConto *et al.*, 2021). Paired with the impact of warming and ocean acidification which diminishes shallow-water coral reefs growth potential (Perry *et al.*, 2018), similar facies configurations as described here are expected to develop in the near future across other carbonate platforms.

Rising sea level is only one of the causes that prevented corals reefs to keep pace with the increasing accommodation. Interestingly, the concept of base level which is well-established for siliciclastic sediments was not really implemented when interpreting the process of carbonate platform drowning. The concept implies that sediments do not necessarily accumulate to sea level, but that a low-lying erosional base (for example, fair-weather wave base, storm-wave base) may be present (Homewood *et al.*, 2000). Deep base level was accepted as an important factor for sedimentation in non-tropical carbonates, as is the case for the ‘shaved shelf’ of South Australia (James *et al.*, 1994; Puga-Bernabéu & Betzler, 2008), where sediments mostly accumulate at water depths below 70 m. In the inner parts of the Bahamas carbonate platform, unfilled accommodation was seen as an important controlling factor of sedimentation (Eberli, 2013; Weij *et al.*, 2019). A base level

lying below sea level has unintentionally been implied by evoking the contribution of the erosive power of ocean currents impinging on carbonate platforms, leading to platform drowning (Isern *et al.*, 2004; Betzler *et al.*, 2009; Eberli *et al.*, 2010; Reolid *et al.*, 2020; Ling *et al.*, 2021) and internal post-drowning unconformities (Mitchell *et al.*, 2015).

Saya de Malha Bank is a further vivid example of how currents control carbonate platform facies and geometry. Lying well within the path of the SEC, the platform is sculptured by this strong current and is swept sediment free in zones with the highest current speed (Fig. 13). There, a hardground forms the seafloor; where current speed relaxes, bioclastic sands develop a ramp-like succession. This means that a deep base level exists in this system. It has been discussed that this platform configuration started during the younger Neogene, hand in hand with the strengthening of the SEC (Betzler *et al.*, 2021). The lesson learned from the Saya de Malha Bank sediment distribution is that current activity is an important controlling factor of lateral carbonate platform facies development.

Internal waves

Southard & Cacchione (1972) demonstrated that internal waves move bottom sediment when shoaling and breaking. Sediment movement is bi-directional along the slope, but downslope transport dominates. Breaking IWs in siliciclastic settings produce sediment waves and ripples at the seafloor (He *et al.*, 2008; Droghei *et al.*, 2016; Ma *et al.*, 2016; Ribó *et al.*, 2016; Reiche *et al.*, 2018; Miramontes *et al.*, 2020) and sculpture erosional truncations, for example along the Mozambique continental margin (Miramontes *et al.*, 2020). In carbonate depositional environments, the effects of IWs on sedimentation were demonstrated to erode the top of drowned carbonate banks (Schlager, 2005) leading to thin pelagic caps on the drowned banks. In shallow-water carbonate settings IWs can regularly transport cold and nutrient-rich waters to the reefs (Wolanski & Delesalle, 1995; Leichter *et al.*, 1998; Wall *et al.*, 2012; DeCarlo *et al.*, 2015; Schmidt *et al.*, 2016; Reid *et al.*, 2019).

At Saya de Malha Bank, the internal waves appear to shape the seafloor in conjunction with the SEC (Fig. 13). The seafloor inclination which is reminiscent of a distally steepened ramp

steepens below the internal wave base. There appears to be sediment winnowing in this area, as indicated by the nepheloid layer in the water column, and sediment coarsening around the area where wave base touches the sediment surface and an erosional scarp developing locally (Fig. 11). The carbonates in this zone are enriched in red algae (Fig. 10) together with some *Halimeda* and LBFs; the water depth of below 100 m is still in the depth range of coralline algae red and green algal growth (Hillis, 2001; Kamenos *et al.*, 2017) but is rather at the lower end for the occurrence of LBFs (Hallock, 1984; Hohenegger, 1994). In shallower areas along the ramp-like profile (Figs 3 and 10) sediments are finer grained and contain less algae and LBFs (Fig. 10). The abundance of the red algae is therefore interpreted to reflect a control of the substrate with low sedimentation rate, especially in the areas of winnowed fines, which are better suited for the encrusting coralline algal growth (Bosence, 1983; Riul *et al.*, 2008; Villas-Boas *et al.*, 2014; Aguirre *et al.*, 2017).

Sediment remobilized by internal waves on Saya de Malha Bank is moved seaward as expressed by the distribution of the nepheloid layer; boluses with sediment transported to shallower waters (Bourgault *et al.*, 2014) are not observed in the data (Figs 10 and 11). Low-angle trough cross-bedding characterizes the area at and just below internal wave base, whereas a directional sediment transport is indicated in deeper waters where submarine dunes have clear foresets. Taken together, these bedforms are therefore interpreted to reflect sediment remobilization and re-distribution by the breaking IWs and the corresponding backflow, with a stronger influence of the east to west flowing SEC in deeper parts, where dune crests are oriented north – south (Fig. 12).

CONCLUSIONS

The Saya de Malha Bank is a large and isolated tropical carbonate platform with mesophotic coralline reefs, rhodolith flats, bioclastic sands and a hardground. Such facies are known to be the main constituents of carbonate-platform drowning sequences, but the bank provides an example where these facies co-exist and form a morphology-dependent and current-dependent mosaic. The hardground is located where the South Equatorial Current sweeps over the bank

top, more current-protected areas display extended flats covered with bioclastic sand and foraminifer–pteropod muds. Mesophotic coralgal reefs and rhodolith beds mostly develop along the margins of the bank, in zones with lower ocean current velocity, or as isolated bodies in the bank's interior. Internal waves impinge onto the southern part of the platform winnowing sediments, and result in large-scale and low-angle submarine dunes. Saya de Malha Bank, therefore, is a natural laboratory which may serve as an analogue to better understand the sedimentological expression of a carbonate platform drowning in the geological record, especially for cases of bank drowning during the Neogene. It also provides the first documented example of the interaction of internal waves (IWs) and sedimentation along a carbonate bank. The tangible effects of the IWs on sedimentation on this carbonate platform are sediment winnowing at the internal wave base, the development of low-angle bedforms below this level, and shaping of a distally steepened ramp morphology. The steepened part of this ramp is where the internal waves induce bottom currents.

ACKNOWLEDGEMENTS

The Bundesministerium für Bildung und Forschung funded the cruise SO270 and post-cruise work through Grant 03G0270A to CB. José Da Silva and Andrian New provided the georeferenced SAR data shown in Fig. 2. Ilona Schutter is thanked for her work within the project MASCARA, Oliver Eisermann helped with the acquisition and processing of the OFOS images. The Joint Commission of the Extended Continental Shelf Mascarene Plateau Region is thanked for allowing work in the JMA and the Department for Continental Shelf, Maritime Zones Administration & Exploration (Mauritius) allowed work in the Republic of Mauritius EEZ. HALLIBURTON-LANDMARK, SCHLUMBERGER and CEGAL Geosciences provided university grants for the seismic processing software PROMAX and seismic interpretation software PETREL as well as its BLUEBACK plugin. The constructive reviews of Stephan Jorry and an anonymous reviewer, and the helpful comments of AE Jody Webster which gave us the chance to sharpen the manuscript are greatly appreciated. Open Access funding enabled and organized by Projekt DEAL.

CONFLICT OF INTEREST

All authors declare that there is no conflict of interest.

DATA AVAILABILITY STATEMENT

The ADCP data have been submitted to the Pangea database in summer 2021. A DOI is currently under preparation. Multibeam, Parasound, seismic and sedimentological data are available from the corresponding author upon reasonable request.

REFERENCES

- Aguirre, J., Braga, J.C. and Bassi, D. (2017) Rhodoliths and rhodolith beds in the rock record. In: *Rhodolith/Maerl Beds: A Global Perspective* (Eds Riosmena-Rodriguez, R., Nelson, W. and Aguirre, J.), Vol. 15, pp. 105–138. Springer, Coastal Research Library, Basel.
- Amado-Filho, G.M., Moura, R.L., Bastos, A.C., Salgado, L.T., Sumida, P.Y., Guth, A.Z., Francini-Filho, R.B., Pereira-Filho, G.H., Abrantes, D.P., Brasileiro, P.S., Bahia, R.G., Leal, R.N., Kaufman, L., Kleypas, J.A., Farina, M. and Thompson, F.L. (2012) Rhodolith beds are major CaCO₃ bio-factories in the tropical south West Atlantic. *PLOS ONE*, 7, e35171.
- Betzler, C., Hübscher, C., Lindhorst, S., Reijmer, J.J.G., Römer, M., Droxler, A.W., Fürstenau, J. and Lüdmann, T. (2009) Monsoonal-induced partial carbonate platform drowning (Maldives, Indian Ocean). *Geology*, 37, 867–870.
- Betzler, C., Lindhorst, S., Lüdmann, T., Reijmer, J.J., Braga, J.-C., Bialik, O.M., Reolid, J., Eisermann, J.O., Emeis, K., Rixen, T. and Bissessur, D. (2021) Current and sea level control the demise of shallow carbonate production on a tropical bank (Saya de Malha Bank, Indian Ocean). *Geology*, 49, 1431–1435.
- Bialik, O.M., Samankassou, E., Meilijson, A., Waldmann, N.D., Steinberg, J., Karcz, K. and Makovsky, Y. (2021) Short-lived early Cenomanian volcanic atolls of mt. Carmel, northern Israel. *Sed. Geol.*, 411, 105805.
- Blomeier, D.P.G. and Reijmer, J.J.G. (1999) Drowning of a lower Jurassic carbonate platform: Jbel Bou Dahar, high atlas, Morocco. *Facies*, 41, 81–110.
- Bosence, D.W.J. (1983) The occurrence and ecology of recent rhodoliths – a review. In: *Coated Grains* (Ed. Peryt, T.M.), pp. 225–242. Springer, Berlin.
- Bosscher, H. and Schlager, W. (1992) Computer simulation of reef growth. *Sedimentology*, 39, 503–512.
- Bourgault, D., Morsilli, M., Richards, C., Neumeier, U. and Kelley, D.E. (2014) Sediment resuspension and nepheloid layers induced by long internal solitary waves shoaling orthogonally on uniform slopes. *Cont. Shelf Res.*, 72, 21–33.
- da Silva, J.C.B., Buijsman, M.C. and Magalhaes, J.M. (2015) Internal waves on the upstream side of a large sill of the Mascarene ridge: a comprehensive view of their generation mechanisms and evolution. *Deep-Sea Res. I Oceanogr. Res. Pap.*, 99, 87–104.

- da Silva, J.C.B., New, A.L. and Magalhaes, J.M. (2011) On the structure and propagation of internal solitary waves generated at the Mascarene plateau in the Indian Ocean. *Deep-Sea Res. I Oceanogr. Res. Pap.*, **58**, 229–240.
- DeCarlo, T.M., Karneckas, K.B., Davis, K.A. and Wong, G.T.F. (2015) Climate modulates internal wave activity in the northern South China Sea. *Geophys. Res. Lett.*, **42**, 831–838.
- DeConto, R.M., Pollard, D., Alley, R.B., Velicogna, I., Gasson, E., Gomez, N., Sadai, S., Condron, A., Gilford, D.M., Ashe, E.L., Kopp, R.E., Li, D. and Dutton, A. (2021) The Paris climate agreement and future sea-level rise from Antarctica. *Nature*, **593**, 83–89.
- Droghei, R., Falcini, F., Casalbore, D., Martorelli, E., Mosetti, R., Sannino, G., Santoleri, R. and Chiocci, F.L. (2016) The role of internal solitary waves on deep-water sedimentary processes: the case of up-slope migrating sediment waves off the Messina Strait. *Sci. Rep.*, **6**, 36376.
- Droxler, A.W. and Jorry, S.J. (2021) The origin of modern atolls: challenging Darwin's deeply ingrained theory. *Ann. Rev. Mar. Sci.*, **13**, 537–573.
- Duncan, R.A. and Hargraves, R.B. (1990) 40AR/39Ar geochronology of basement rocks from the Mascarene Plateau, the Chagos Bank and the Maldives Ridge. In: *Proceedings of the Ocean Drilling Project, Science Results 1990* (Eds Duncan, R.A., Backman, J. and Peterson, I.C.), Vol. **115**, pp. 43–51. Ocean Drilling Program, Texas A&M University, College Station.
- Eberli, G.P. (2013) The uncertainties involved in extracting amplitude and frequency of orbitally driven sea-level fluctuations from shallow-water carbonate cycles. *Sedimentology*, **60**, 64–84.
- Eberli, G.P., Anselmetti, F.S., Isern, A.R. and Delius, H. (2010) Timing of changes in sea level and currents along Miocene platforms on the Marion plateau. In: *Cenozoic Carbonate Systems of Australasia* (Eds Morgan, W.A., George, A.D., Harris, P.M., Kupecz, J.A. and Sarg, J.F.), *SEPM Spec. Pub.*, Vol. **95**, pp. 219–242. Society for Sedimentary Geology, Tulsa.
- Erlich, R.N., Barrett, S.F. and Ju, G.B. (1990) Seismic and geologic characteristics of drowning events on carbonate platforms. *Am. Assoc. Petrol. Geol. Bull.*, **74**, 1523–1537.
- Fedorov, V.V., Rubinsteyn, I.G., Danilov, I.V. and Lanin, V.I. (1980) Bottom landscapes of Saya de Malha Bank in the Indian Ocean. *Oceanology*, **20**, 434–439.
- Feng, M. and Wijffels, S. (2002) Intraseasonal variability in the south equatorial current of the East Indian Ocean. *J. Phys. Oceanogr.*, **32**, 265–277.
- Fyhn, M.B.W., Boldreel, L.O., Nielsen, L.H., Giang, T.C., Nga, L.H., Hong, N.T.M., Nguyen, N.D. and Abatzis, I. (2013) Carbonate platform growth and demise offshore Central Vietnam: effects of early Miocene transgression and subsequent onshore uplift. *J. Asian Earth Sci.*, **76**, 152–168.
- Hallock, P. (1984) Distribution of selected species of living algal symbiont-bearing foraminifera on two Pacific coral reefs. *J. Foram. Res.*, **14**, 250–261.
- Hallock, P. and Schlager, W. (1986) Nutrient excess and the demise of coral reefs and carbonate platform. *Palaios*, **1**, 389–398.
- Harris, P.T., Heap, A.D., Wassenberg, T. and Passlow, V. (2004) Submerged coral reefs in the Gulf of Carpentaria, Australia. *Mar. Geol.*, **207**, 185–191.
- He, Y., Gao, Z., Luo, J., Luo, S. and Liu, X. (2008) Characteristics of internal-wave and internal-tide deposits and their hydrocarbon potential. *Petrol. Sci.*, **5**, 37–44.
- Hillis, L.W. (2001) The calcareous reef alga Halimeda (Chlorophyta, Byrpsidales): a cretaceous genus that diversified in the cenozoic. *Palaeogeogr. Palaeoclimatol. Palaeoecol.*, **166**, 89–100.
- Hohenegger, J. (1994) Distribution of living larger foraminifera NW of Sesoko-Jima, Okinawa, Japan. *Marine Ecol.*, **15**, 291–334.
- Homewood, P., Mauriaud, P. and Lafont, F. (2000) Best practices in sequence stratigraphy for explorationists and reservoir engineers. *Bull. Cent. Rech. Explor. Prod. Elf-Aquitaine, Mem.*, **25**, 81.
- Isern, A., Anselmetti, F.S. and Blum, P. (2004) A Neogene carbonate platform, slope and shelf edifice shaped by sea level and ocean currents, Marion plateau (Northeast Australia). In: *Seismic Imaging of Carbonate Reservoirs and Systems* (Eds Eberli, G.P., Masafello, J.L. and Sarg, J.F.), *AAPG Mem.*, Vol. **81**, pp. 291–307. The American Association of Petroleum Geologists, Tulsa.
- James, N.P., Boreen, T.D. and Feary, D.A. (1994) Holocene carbonate sedimentation on the west Eucla shelf, great Australian bight: a shaved shelf. *Sediment. Geol.*, **90**, 161–177.
- Jenkyns, H.C. and Wilson, P.A. (1999) Stratigraphy, paleoceanography, and evolution of cretaceous pacific guyots: relics from a greenhouse earth. *Am. J. Sci.*, **299**, 341–392.
- Kamenos, N.A., Burdett, H.L. and Darrenougue, N. (2017) Coralline algae as recorders of past climatic and environmental conditions. In: *Rhodolith/Maerl Beds: A Global Perspective* (Eds Riosmena-Rodríguez, R., Nelson, W. and Aguirre, J.), pp. 27–53. Springer, Berlin.
- Kendall, C.G.S.C. and Schlager, W. (1981) Carbonates and relative changes in sea level. *Mar. Geol.*, **44**, 181–212.
- Konyaev, K.V., Sabinin, K.D. and Serebryany, A.N. (1995) Large-amplitude internal waves at the Mascarene ridge in the Indian Ocean. *Deep-Sea Res. I Oceanogr. Res. Pap.*, **42**, 2075–2091.
- Leichter, J.J., Shellenbarger, G., Genovese, S.J. and Wing, S.R. (1998) Breaking internal waves on a Florida (USA) coral reef: a plankton pump at work? *Mar. Ecol. Prog. Ser.*, **166**, 83–97.
- Lindhorst, S., Appoo, J., Artschwager, M., Bialik, O., Birkicht, M., Bissessur, D., Braga, J.-C., Budke, L., Bunzel, D., Coopen, P., Eberhardt, B., Eggers, D., Eisermann, J.O., El Gareb, F., Emeis, K., Gebner, A.-L., Hüge, F., Knaack-Völker, H., Kornrumpf, N., Lenz, N., Lüdmann, T., Metzke, M., Naderipour, C., Neziraj, G., Reijmer, J., Reolid, J., Reule, N., Rixen, T., Saitz, Y., Schäfer, W., Schutter, I., Siddiqui, C., Sorry, A., Taphorn, B., Vosen, S., Wasilewski, T. and Welsch, A. (2019) *Saya de Malha Carbonates, Oceanography and Biogeochemistry (Western Indian Ocean) Cruise No. SO270, 2019-09-06 - 2019-10-23, Hong Kong (China) - Port Louis (Mauritius) (Englisch)*. SONNE-Berichte, SO270. Gutachterpanel Forschungsschiffe, Bonn, p. 102. Gutachterpanel Forschungsschiffe, Bonn. https://doi.org/10.2312/cr_so270
- Ling, A., Eberli, G.P., Swart, P.K., Reolid, J., Stainbank, S., Rüggeberg, A. and Betzler, C. (2021) Middle Miocene platform drowning in the Maldives associated with monsoon-related intensification of currents. *Palaeogeogr. Palaeoclimatol. Palaeoecol.*, **567**, 110275.
- Ma, X., Yan, J., Hou, Y., Lin, F. and Zheng, X. (2016) Footprints of obliquely incident internal solitary waves and internal tides near the shelf break in the northern South China Sea. *J. Geophys. Res. Oceans*, **121**, 8706–8719.

- Marino, M. and Santantonio, M.** (2010) Understanding the geological record of carbonate platform drowning across rifted Tethyan margins: examples from the lower Jurassic of the Apennines and Sicily (Italy). *Sed. Geol.*, **225**, 116–137.
- Meyerhoff, A.A. and Kamen-Kaye, M.** (1981) Petroleum prospects of Saya de Malha and Nazareth banks, Indian Ocean. *AAPG Bull.*, **65**, 1344–1347.
- Miramontes, E., Jouet, G., Thereau, E., Bruno, M., Penven, P., Guerin, C., Le Roy, P., Droz, L., Jorry, S.J., Hernández-Molina, F.J., Thiéblemont, A., Silva Jacinto, R. and Cattaneo, A.** (2020) The impact of internal waves on upper continental slopes: insights from the Mozambican margin (Southwest Indian Ocean). *Earth Surf. Process. Landf.*, **45**, 1469–1482.
- Mitchell, N.C., Simmons, H.L. and Lear, C.H.** (2015) Modern and ancient hiatuses in the pelagic caps of Pacific guyots and seamounts and internal tides. *Geosphere*, **11**, 1590–1606.
- Montaggioni, L.** (2005) History of Indo-Pacific coral reef systems since the last glaciation: development patterns and controlling factors. *Earth Sci. Rev.*, **71**, 1–75.
- Montaggioni, L.F. and Martin-Garin, B.** (2020) Quaternary development history of coral reefs from west Indian islands: a review. *Int. J. Earth Sci.*, **109**, 911–930.
- Mutti, M., Droxler, A.W. and Cunningham, A.D.** (2005) Evolution of the northern Nicaragua rise during the Oligocene-Miocene: drowning by environmental factors. *Sed. Geol.*, **175**, 237–258.
- New, A.L., Alderson, S.G., Smeed, D.A. and Stansfield, K.L.** (2007) On the circulation of water masses across the Mascarene plateau in the South Indian Ocean. *Deep-Sea Res. I Oceanogr. Res. Pap.*, **54**, 42–74.
- New, A.L., Magalhaes, J.M. and da Silva, J.C.B.** (2013) Internal solitary waves on the Saya de Malha bank of the Mascarene plateau: SAR observations and interpretation. *Deep-Sea Res. I Oceanogr. Res. Pap.*, **79**, 50–61.
- Paumard, V., Zuckmeyer, E., Boichard, R., Jorry, S.J., Bourget, J., Borgomano, J., Maurin, T. and Ferry, J.-N.** (2017) Evolution of late Oligocene - early Miocene attached and isolated carbonate platforms in a volcanic ridge context (Maldives type), Yadana field, offshore Myanmar. *Mar. Petrol. Geol.*, **81**, 361–387.
- Perry, C.T., Alvarez-Filip, L., Graham, N.A.J., Mumby, P.J., Wilson, S.K., Kench, P.S., Manzello, D.P., Morgan, K.M., Slangen, A.B.A., Thomson, D.P., Januchowski-Hartley, F., Smithers, S.G., Steneck, R.S., Carlson, R., Edinger, E.N., Enochs, I.C., Estrada-Saldívar, N., Haywood, M.D.E., Kolodziej, G., Murphy, G.N., Pérez-Cervantes, E., Suchley, A., Valentino, L., Boenish, R., Wilson, M. and Macdonald, C.** (2018) Loss of coral reef growth capacity to track future increases in sea level. *Nature*, **558**, 396–400.
- Petschick, R.** (2002) Röntgendiffraktometrie in der Sedimentologie. *Schriftenr. Deutsche Geol. Ges.*, **18**, 99–118.
- Puga-Bernabéu, Á. and Betzler, C.** (2008) Cyclicality in Pleistocene upper-slope cool-water carbonates: unravelling sedimentary dynamics in deep-water sediments, great Australian bight, ODP leg 182, site 1131A. *Sed. Geol.*, **205**, 40–52.
- Reiche, S., Hübscher, C., Brenner, S., Betzler, C. and Hall, J.K.** (2018) The role of internal waves in the late quaternary evolution of the Israeli continental slope. *Mar. Geol.*, **406**, 177–192.
- Reid, E.C., DeCarlo, T.M., Cohen, A.L., Wong, G.T.F., Lentz, S.J., Safaie, A., Hall, A. and Davis, K.A.** (2019) Internal waves influence the thermal and nutrient environment on a shallow coral reef. *Limnol. Oceanogr.*, **64**, 1949–1965.
- Reolid, J., Betzler, C., Braga, J.C., Lüdmann, T., Ling, A. and Eberli, G.P.** (2020) Facies and geometry of drowning steps in a Miocene carbonate platform (Maldives). *Palaeogeogr. Palaeoclimatol. Palaeoecol.*, **538**, 109455.
- Ribó, M., Puig, P., Muñoz, A., Lo Iacono, C., Masqué, P., Palanques, A., Acosta, J., Guillén, J. and Gómez Ballesteros, M.** (2016) Morphobathymetric analysis of the large fine-grained sediment waves over the Gulf of Valencia continental slope (NW Mediterranean). *Geomorphology*, **253**, 22–37.
- Riul, P., Targino, C.H., Farias, J.D.N., Visscher, P.T. and Horta, P.A.** (2008) Decrease in Lithothamnion sp. (Rhodophyta) primary production due to the deposition of a thin sediment layer. *J. Mar. Biol. Assoc.*, **88**, 17–19.
- Rosset, S., Wiedenmann, J., Reed, A.J. and D'Angelo, C.** (2017) Phosphate deficiency promotes coral bleaching and is reflected by the ultrastructure of symbiotic dinoflagellates. *Mar. Pollut. Bull.*, **118**, 180–187.
- Sattler, U., Immenhauser, A., Schlager, W. and Zampetti, V.** (2009) Drowning history of a Miocene carbonate platform (Zhujiang formation, South China Sea). *Sed. Geol.*, **219**, 318–331.
- Schlager, W.** (1989) Drowning unconformities on carbonate platforms. In: *Controls on Carbonate Platform and Basin Development* (Eds Crevello, P.D., Wilson, J.L., Sarg, J.F. and Read, J.F.), *SEPM Special Publication*, Vol. **44**, pp. 15–25. Society for Sedimentary Geology, Tulsa.
- Schlager, W.** (1991) Depositional bias and environmental change-important factors in sequence stratigraphy. *Sediment. Geol.*, **70**, 109–130.
- Schlager, W.** (2005) Carbonate sedimentology and sequence stratigraphy. *Concepts Sediment. Paleont.*, **8**, 200.
- Schlager, W. and Camber, O.** (1986) Submarine slope angles, drowning unconformities and self-erosion of limestone escarpments. *Geology*, **14**, 762–765.
- Schmidt, G.M., Wall, M., Taylor, M., Jantzen, C. and Richter, C.** (2016) Large-amplitude internal waves sustain coral health during thermal stress. *Coral Reefs*, **35**, 869–881.
- Southard, J.B. and Cacchione, D.A.** (1972) Experiments on bottom sediment movement by breaking internal waves. In: *Shelf Sediment Transport: Process and Pattern* (Eds Swift, D.J., Duane, D.B. and Pilkey, O.H.), pp. 83–97. Dowden, Hutchinson & Ross, Stroudsburg, PA.
- Strohmeier, C.J., Meyer, L., Yose, L.A., Walley, D.S., Yusoff, M.M., Lyons, D.Y., Sutton, J., Rivers, J.M., Carlo, D., von Schnurbein, B., Zhou, D. and Phong, N.X.** (2020) Reservoir characterization of an isolated middle miocene carbonate platform: ca Voi Xanh field, offshore Vietnam. *J. Petrol. Geol.*, **43**, 5–26.
- Teillet, T., Fournier, F., Montaggioni, L.F., BouDagher-Fadel, M., Borgomano, J., Braga, J.C., Villeneuve, Q. and Hong, F.** (2020) Development patterns of an isolated oligo-mesophotic carbonate buildup, early Miocene, Yadana field, offshore Myanmar. *Mar. Petrol. Geol.*, **111**, 440–460.
- Van der Land, J.** (1977) The Saba Bank - a large atoll in the northeastern Caribbean. *FAO Fish. Rep.*, **200**, 469–481.
- Vecsei, A.** (2000) Database on isolated low-latitude carbonate banks. *Facies*, **43**, 205–222.
- Villas-Boas, A.B., Tãmega, F.T.S., Coutinho, M.A.R. and Figueiredo, M.A.O.** (2014) Experimental effects of sediment burial and light attenuation on two coralline algae of a deep water rhodolith bed in Rio de Janeiro, Brazil. *Cryptogam. Algal.*, **35**, 67–76.

- Vortsepneva, E.** (2008) Saya de Malha Bank – an invisible island in the Indian Ocean, pp. 44, <https://lighthouse-foundation.org/Binaries/Binary1070/Saya-de-Malha-report-final.pdf>.
- Wall, M., Schmidt, G.M., Janjang, P., Khokiattiwong, S. and Richter, C.** (2012) Differential impact of monsoon and large amplitude internal waves on coral reef development in the Andaman Sea. *PLoS ONE*, **7**, e50207.
- Weij, R., Reijmer, J.J.G., Eberli, G.P. and Swart, P.K.** (2019) The limited link between accommodation space, sediment thickness, and inner platform facies distribution (Holocene–Pleistocene, Bahamas). *Depositional Rec.*, **5**, 400–420.
- Wienberg, C., Westphal, H., Kwohl, E. and Hebbeln, D.** (2010) An isolated carbonate knoll in the Timor Sea (Sahul shelf, NW Australia): facies zonation and sediment composition. *Facies*, **56**, 179–193.
- Wilson, P.A., Jenkyns, H.C., Elderfield, H. and Larson, R.L.** (1998) The paradox of drowned carbonate platforms and the origin of cretaceous Pacific guyots. *Nature*, **392**, 889–894.
- Wolanski, E. and Delesalle, B.** (1995) Upwelling by internal waves, Tahiti, French Polynesia. *Cont. Shelf Res.*, **15**, 357–368.
- Zempolich, W.G.** (1993) The drowning succession in Jurassic carbonates of the venetian Alps, Italy: a record of supercontinent breakup, gradual eustatic rise, and eutrophication of shallow-water environments. In: *Carbonate Sequence Stratigraphy* (Eds Loucks, R.G. and Sarg, J.F.), *Am. Assoc. Petrol. Geol. Mem.*, Vol. **57**, pp. 63–105. The American Association of Petroleum Geologists, Tulsa.
- Zinke, J., Reijmer, J.J.G., Taviani, M., Dullo, W.-C. and Thomassin, B.** (2005) Facies and faunal assemblage changes in response to the Holocene transgression in the lagoon of Mayotte (Comoro archipelago, SW Indian Ocean). *Facies*, **50**, 391–408.

Manuscript received 27 December 2021; revision accepted 10 August 2022

Supporting Information

Additional information may be found in the online version of this article:

Appendix S1. West – east cross-section through Saya de Malha Bank (location of Section a is shown in Fig. 1) with distribution of main components in the size fraction above 2 mm. Numbers refer to stations (see Fig. 1 for location).

Appendix S2. West – east cross-section through Saya de Malha Bank (location of Section a is shown in Fig. 1) with distribution of main components in the size fraction 0.5 to 2.0 mm. Numbers refer to stations (see Fig. 1 for location).

Appendix S3. West – east cross-section through Saya de Malha Bank (location of Section b is shown in Fig. 1) with distribution of main components in the size fraction above 2 mm. Numbers refer to stations (see Fig. 1 for location). PS019 indicates intersection of Section c.

Appendix S4. West – east cross section through Saya de Malha Bank (location of Section b is shown in Fig. 1) with distribution of main components in the size fraction 0.5 to 2.0 mm. Numbers refer to stations (see Fig. 1 for location). PS019 indicates intersection of Section c.

Appendix S5. North-east – south-west cross-section through Saya de Malha Bank (location of Section c is shown in Fig. 1) with distribution of main components in the size fraction above 2 mm. Numbers refer to stations (see Fig. 1 for location). PS001 indicates intersection of Section b.

Appendix S6. North-east – south-west cross-section through Saya de Malha Bank (location of Section c is shown in Fig. 1) with distribution of main components in the size fraction 0.5 to 2.0 mm. Numbers refer to stations (see Fig. 1 for location). PS001 indicates intersection of Section b.

Appendix S7. Supplementary Material.